AD

# Destruction of Isotropic and Anisotropic Materials at Impact—Wave Loading

Final Technical Report
by

A.V. Radchenko, M.N. Krivosheina, S.V. Kobenko, V.F. Tolkachev
(June 2001)

United States Army

EUROPEAN RESEARCH OFFICE OF THE U.S. ARMY

London, England

CONTRACT NUMBER N68171-00-M-5806

R&D 8573-AN-01S

Russian Academy of Sciences, Siberian Branch, Tomsk Scientific Centre
Department for Structural Macrokinetics

# REPORT DOCUMENTATION PAGE

Form Approved
OMB NO. 0704-0188



| 1. AGENCY USE ONLY ( Leave Blank) | 2. REPORT DATE | 3. REPORT TYPE AND DATES COVERED |
|---|---|---|
| | August 2001 | Final, June 00 - June 01 |

4. TITLE AND SUBTITLE

Destruction of Isotropic and Anisotropic Materials at Impact—Wave Loading

5. FUNDING NUMBERS

C N68171-00-M-5806

6. AUTHOR(S)

A.V. Radchenko, M.N. Krivosheina, S.V. Kobenko, V.F. Tolkachev

7. PERFORMING ORGANIZATION NAME(S) AND ADDRESS(ES)

Russian Academy of Sciences, Siberian Branch, Tomsk Scientific Centre
Department for Structural Macrokinetics
10/3 Akademichesky Ave., 634055, Tomsk, Russia

8. PERFORMING ORGANIZATION REPORT NUMBER

C N68171-00-M-5806/01-4

9. SPONSORING / MONITORING AGENCY NAME(S) AND ADDRESS(ES)

European Research Office
USARDSG-UK, Old Marylebone Road, London, NW1 5TH, England

10. SPONSORING / MONITORING AGENCY REPORT NUMBER

11. SUPPLEMENTARY NOTES

12 a. DISTRIBUTION / AVAILABILITY STATEMENT.

12 b. DISTRIBUTION CODE

13. ABSTRACT (Maximum 200 words)

Comparative analysis of behaviour of anisotropic and isotropic materials at normal and oblique impact was conducted. Modeling of materials behaviour was conducted in the framework of phenomenological approach by method of finite elements. To describe the failure of investigated materials was used tensor-polynomial criterion of the forth degree. The adequacy of the model used is tested by experimental investigation. Plates out of transtropic organoplastic were used as anisotropic samples. Isotropic samples are plates out of isotropic glass-plastic. Impact loading of plates was realized with the use of compact steel cylinder. The comparison of results of numerical modeling and experimental data was made according to integral process parameters: residual striker's velocity, striker's deformation after punching of plates (residual striker's length) and profile of stress. In the framework of the phenomenological approach the influence of orientation of elastic and strength properties of the orthotropic material on fracture was investigated. The analysis of dynamics of interaction between the striker and plates showed qualitative differences in the evolution on failure of isotropic and anisotropic materials. This distinction is due not only to various values of strength parameters, but also to various velocities of propagation of shock wave and relief waves in anisotropic materials in different directions.

14. SUBJECT TERMS

anisotropic material, impact, shock wave, relief wave, model, striker, velocity, failure, stress

15. NUMBER OF PAGES
38

16. PRICE CODE

| 17. SECURITY CLASSIFICATION OF REPORT | 18. SECURITY CLASSIFICATION ON THIS PAGE | 19. SECURITY CLASSIFICATION OF ABSTRACT | 20. LIMITATION OF ABSTRACT |
|---|---|---|---|
| UNCLASSIFIED | UNCLASSIFIED | UNCLASSIFIED | UL |

NSN 7540-01-280-5500

Standard Form 298 (Rev.2-89)
Prescribed by ANSI Std. 239-18

298-102

## ABSTRACT

Comparative analysis of behaviour of anisotropic and isotropic materials at normal and oblique impact was conducted. Modeling of materials behaviour was conducted in the framework of phenomenological approach by method of finite elements. To describe the failure of investigated materials was used tensor-polynomial criterion of the forth degree. The adequacy of the model used is tested by experimental investigation. Plates out of transtropic organoplastic were used as anisotropic samples. Isotropic samples are plates out of isotropic glass-plastic. Impact loading of plates was realized with the use of compact steel cylinder. The comparison of results of numerical modeling and experimental data was made according to integral process parameters: residual striker's velocity, striker's deformation after punching of plates (residual striker's length) and profile of stress. In the framework of the phenomenological approach the influence of orientation of elastic and strength properties of the orthotropic material on fracture was investigated. The analysis of dynamics of interaction between the striker and plates showed qualitative differences in the evolution on failure of isotropic and anisotropic materials. This distinction is due not only to various values of strength parameters, but also to various velocities of propagation of shock wave and relief waves in anisotropic materials in different directions.

# Table of Contents

## 1 INTRODUCTION

At present, the wide application of the materials with preset directivity of properties in various fields of engineering defines the increased interest to the investigations of anisotropic materials behavior under various conditions. But in Russia as well as abroad such investigations are conducted mainly for static conditions. The behavior of anisotropic materials under dynamic loads is practically not investigated. This is especially the case with experimental investigations as well as with mathematical and numerical modeling. The impact interaction of the solids in a wide range of kinematic and geometric conditions is the complex problem of mechanics. The difficulties, connected with the theoretic study of the destruction and deformation of materials on impact by analytical methods force to introduce member of simplifying hypothesis which distort the real picture in majority of cases. In this connection it should be accepted that the leading role in the investigation of phenomena, connected with high-speed interaction of solids belongs to the experimental and numeric investigations at present. The investigations of the material damage under impact show that the destruction mechanisms change with the interaction conditions. The experiments strongly testifiers that in a number of case the resulting destruction is determined by the combination of several mechanisms. But in the experiments we fail to trace sequence, operation time and the contribution of various destruction mechanisms. Besides, the distractions, obtained at the initial stages of the process can't always be identified in the analysis of the resulting destruction of the materials. For anisotropic materials the strength itself is multivalued and uncertain notion due to the polymorphism of behavior of these materials under the load. The limiting state of anisotropic bodies may be of different physical nature in dependence on load orientation, stressed state type and other factors. The dependence of the physical nature of limiting states is revealed in the sturdy of the experimental data. The investigations of hydrostatic pressure effect upon the strength of isotropic materials show that comprehensively the compression exerts a weak action on the resistance of isotropic materials under static loads. Therefore, the classic theories of strength, plasticity and creep are based on assumption about the lack of the effect of fall stress tensor upon strength isotropic materials. In the experiments with anisotropic materials it was state that flow phenomenon may arise only under the action of hydrostatic pressure. Upon the materials, strength is due to the anisotropy. The shape of anisotropic bodies changes under the action of hydrostatic pressure. If these changes reach such values that, they don't disappear under relief, the limiting state should come. Therefore, the postulate of classic strength that hydrostatic pressure can't transfer the material to the dangerous state is not valid for anisotropic materials. The phenomenological approach to the investigation of the dynamics of deformation and destruction of anisotropic and isotropic materials is used in the project. The phenomenological approach to the materials strength requires that the conditions of the transition into the limiting state of various physical natures should be determinated by one equation (criterion). The necessity of such an approach results from destruction polymorphism, being deduced experimentally. For anisotropic bodies the phenomenological approach has many advantages, since there appears the possibility to use general condition of strength for the material different in composition and technology but similar in symmetry of properties, and also for the materials with substantial anisotropy, for which one and the same stressed state can result in limiting conditions, different in physical nature.

## 2 THE BASIC EQUATIONS OF THE MODEL

The system of equations describing non-stationary adiabatic movements of compressing medium in the arbitrary coordinate system (i=1,2,3) includes the following equations:
-continuity equation:

$$\frac{\partial \rho}{\partial t} + \mathrm{div}\rho\bar{\upsilon} = 0 \qquad (2.1)$$

-eqations of motion:

$$\rho a^k = \nabla_i \sigma^{ki} + F^k \qquad (2.2)$$

where

$$\sigma^{ki} = -p\delta_{ki} + S^{ki}\ ;\ \nabla_i \sigma^{ki} = \sigma^{ki}_{,i} + \sigma^{mi}\Gamma^k_{mi} + \sigma^{ki}\Gamma^m_{mi}$$

$$a^k = \frac{\partial \upsilon^k}{\partial t} + \upsilon^i \nabla_i \upsilon^k$$

-equation of energy:

$$\frac{dE}{dt} = \frac{1}{\rho}\sigma^{ij} e_{ij}. \qquad (2.3)$$

Here $\rho$ is the medium density; $\bar{\upsilon}$ is the speed vector; $a^k$ are the components of acceleration vector; $F^k$ are the components of vector of mass forces; $\Gamma^k_{ij}$ are Kristoffel symbols; $\delta_{ij}$ is the Kronekker symbol; $\sigma^{ij}$, $S^{ij}$ and P are contravariant components of the symmetrical tensor of stress, deviator of stress and the ballpart of tensor of stress-pressure, respectively; E is the specific internal energy; $e_{ij}$ are the components of the symmetric tensor of strain rates:

$$e_{ij} = \frac{1}{2}\left(\nabla_i \upsilon_j + \nabla_j \upsilon_i\right). \qquad (2.4)$$

Supposing that the principal of minimum work of true stress at the increment in plastic deformations is valid for the medium, let's write the relation of the component of tensor of strain rates and stress deviator for the strike material in the form of

$$2G\left(e_{ij} - \frac{1}{3}e_{kk}\delta_{ij}\right) = \frac{DS^{ij}}{Dt} + \lambda S^{ij}, (\lambda \geq 0). \qquad (2.5)$$

Here

$$\frac{DS^{ij}}{Dt} = \frac{dS^{ij}}{dt} - S^{ik}\omega_{jk} - S^{jk}\omega_{ik}$$

where $\omega_{ij} = \frac{1}{2}\left(\nabla_i \upsilon_j - \nabla_j \upsilon_i\right)$, G is shear modulus.

Under elastic deformation the parameter $\lambda = 0$ and under plastic deformation ($\lambda > 0$) is defined with the help of Von Mises law:

$$S^{ij}S_{ij} = \frac{2}{3}\sigma_d^2 \tag{2.6}$$

where $\sigma_d$ is the dynamic yield point.

The pressure in the material of the striker was present by the function of the specific internal energy ( E ) and density ( $\rho$ ):

$$P = P(\rho, E) \tag{2.7}$$

The equation of Mie-Gruneisen type [1] and wide-range equation [2] were used and equation of state (2.7). The components of tensor of stress in the barrier material before the destruction are defined from relations for orthotropic body:

$$\begin{aligned}
&\frac{d\sigma_{11}}{dt} = C_{11}e_{11} + C_{12}e_{22} + C_{13}e_{33}, \ \frac{d\sigma_{12}}{dt} = C_{44}e_{12}, \ \frac{d\sigma_{13}}{dt} = C_{66}e_{13}, \\
&\frac{d\sigma_{22}}{dt} = C_{12}e_{11} + C_{22}e_{22} + C_{23}e_{33}, \ \frac{d\sigma_{23}}{dt} = C_{55}e_{23}, \\
&\frac{d\sigma_{33}}{dt} = C_{13}e_{11} + C_{23}e_{22} + C_{33}e_{33}
\end{aligned} \tag{2.8}$$

where, $C_{ij}$ are elastic constants.

The elastic constants $C_{ij}$ can be expressed through Young's modulus $E_i$, shift modulus $G_{ij}$ and Poisson's ratio $\nu_{ij}$:

$$\begin{aligned}
&C_{11} = \frac{1}{E_2 A}\left(\frac{1}{E_3} - \frac{\nu_{23}^2}{E_2}\right); C_{12} = \frac{1}{E_3 A}\left(\frac{\nu_{31}\nu_{23}}{E_3} + \frac{\nu_{12}}{E_1}\right); C_{13} = \frac{1}{E_2 A}\left(\frac{\nu_{12}\nu_{23}}{E_1} + \frac{\nu_{31}}{E_3}\right) \\
&C_{22} = \frac{1}{E_3 A}\left(\frac{1}{E_1} - \frac{\nu_{31}^2}{E_3}\right); C_{23} = \frac{1}{E_1 A}\left(\frac{\nu_{12}\nu_{31}}{E_3} + \frac{\nu_{23}}{E_2}\right); C_{33} = \frac{1}{E_1 A}\left(\frac{1}{E_2} - \frac{\nu_{12}^2}{E_1}\right) \\
&C_{44} = G_{12}; C_{55} = G_{23}; C_{66} = G_{13} \\
&A = \frac{1}{E_1 E_2 E_3}\left(1 - 2\nu_{12}\nu_{23}\nu_{31} - \frac{E_1}{E_3}\nu_{31}^2 - \frac{E_2}{E_1}\nu_{12}^2 - \frac{E_3}{E_2}\nu_{23}^2\right)
\end{aligned} \tag{2.9}$$

Tensor-polynomial criterion of the fourth degree [3-8, 18], taking in to account the hydrostatic pressure is used to define the transition of the barrier material into the destructed state:

$$\alpha_{ik\ell m}\sigma_{ik}\sigma_{\ell m} - \left[\frac{\left(\sigma_{ik}\delta_{ik}\right)^2 + \sigma_{ik}\sigma_{ik}}{2}\right]^{\frac{1}{2}} \le 0 \tag{2.10}$$

In complex stressed states that tensor-polynomial criterion contains stresses to the second and fourth power; the fourth order of polynomial allows not only to approximate the experimental data better than the second one but also comply with the nature of strongly anisotropic bodies: the strength surface for strongly anisotropic bodies may contain vortex as well as concave sites according to the different character of dangerous state at these sites.

The first summand ($\alpha_{ik\acute{e}m}\sigma_{ik}\sigma_{\acute{e}m}$) is the joint invariant of stress tensor and strength tensor, and the second one expresses the dependence of strength of anisotropic bodies upon two invariants of stress tensor $J_1$ and $J_2$. The first summand of this equation is the "plastic potential'' in its extended form. In physical aspect the invariant equation may be considered as the generalization of Mises "plastic potential" for the case when clear dependence of limiting state upon the first invariant of stress tensor (upon hydrostatic pressure $J_1$) takes place. In completely extended form the criterion (2.10) is the polynomial of the forth power regarding to the six components of operating stresses. The constants $\alpha_{ik\acute{e}m}$ are (in the Equation (2.10)) the components of the forth range i.e. strength tensor.

It is supposed that the destruction of anisotropic material under the conditions of heavy dynamic loads occurs according to the following scheme:

1. if the Equation (2.10) is disturbed under condition of material compression ($e_{kk} \le 0$), the material looses its anisotropic properties and its behavior is described by isotropic hydrodynamic model, retaining only compressive strength;
2. if the Equation (2.10) is disturbed under tension conditions ($e_{kk} > 0$), the material is believed to be failed completely and components of stress tensor are equal to zero.

In the cartesian coordinate system XYZ (1 corresponds to the axis X, 2 - Y, 3 - Z) the criterion (2.10) for the orthotropic body can be written as:

$$\frac{\sigma_x^2 + c\sigma_y^2 + b\sigma_z^2 + d\tau_{xy}^2 + p\tau_{yz}^2 + r\tau_{xz}^2 + s\sigma_x\sigma_y + t\sigma_y\sigma_z + f\sigma_x\sigma_z}{\sqrt{\sigma_x^2 + \sigma_y^2 + \sigma_z^2 + \tau_{xy}^2 + \tau_{yz}^2 + \tau_{xz}^2 + \sigma_x\sigma_y + \sigma_y\sigma_z + \sigma_x\sigma_z}} \le [\sigma_0] \qquad (2.11)$$

where

$$[\sigma_0] = \frac{\sigma_{bx}}{k_b};\ c = \frac{\sigma_{bx}}{\sigma_{by}};\ b = \frac{\sigma_{bx}}{\sigma_{bz}};\ d = \frac{\sigma_{bx}}{\tau_{bxy}};\ p = \frac{\sigma_{bx}}{\tau_{byz}};\ r = \frac{\sigma_{bx}}{\tau_{bxz}};\ s = \frac{4\sigma_{bx}}{\sigma_{bxy}^{(45)}} - c - d - 1;$$

$$t = \frac{4\sigma_{bx}}{\sigma_{byz}^{(45)}} - c - b - p;\ f = \frac{4\sigma_{bx}}{\sigma_{bzx}^{(45)}} - b - r - 1.$$

Here $\sigma_x, \sigma_y, \sigma_z$ and $\tau_{xy}, \tau_{xz}, \tau_{yz}$ are normal and shear components of the stress tensor. The letter $\sigma$ with the low symbol "b " defines the value of dangerous stress (strength limit) at the tension or compression in the axis direction, corresponding to the second low index; the letter $\tau$ defines the same thing at pure shear, at which the right angle is changed between the axes, indicated in the index. The upper index (45) at the letter $\sigma$ indicates the strength limit in the diagonal direction (at the angle of 45° to the symmetry axes), located in the plane, corresponding to the low indexes.

## 3 INVESTIGATION RESULTS

### 3.1 Research of features of behaviour isotropic and anisotropic of materials under impact. Comparison of numerical and experimental results

We shall consider the interaction of the steel strikes with isotropic and anisotropic barrier in a general, three-dimensional case in the cartesian coordinate system XYZ (Figure 1). The striker is the compact cylinder, occupying the $D_1$ region, and limited by the surfaces $\Sigma_1$ and $\Sigma_2$. At the starting moment the speed vector of the striker coincides with its symmetry axis and forms the angle $\alpha$ with the normal to the barrier. The barrier occupies the $D_2$ region and it is limited by the $\Sigma_2$ and $\Sigma_3$ surfaces. The $\Sigma_1$ and $\Sigma_3$ surfaces are free from the forces, $\Sigma_2$ is the contact surface of the cylinder with the plate.

For the Equations (2.1-2.11), the problem with the initial (at t=0) and present (at the $\Sigma_1$, $\Sigma_2$, $\Sigma_3$ surfaces) boundary conditions is proposed.

Initial conditions ( $t = 0$ ):

$$\sigma_i=\tau_{ij}=E=u=0 \text{ at } (x,y,z)\in D_1 \cup D_2,\ i,j=x,y,z \tag{3.1}$$

$$u = \upsilon_0\sin(\alpha);\ w = \upsilon_0\cos(\alpha);\ \upsilon=0 \text{ at } (x,y,z)\in D_1 \tag{3.2}$$

$$u=\upsilon=w=0 \text{ at } (x,y,z)\in D_2 \tag{3.3}$$

$$\rho=\rho_i \text{ at } (x,y,z)\in D_i,\ i=1,2. \tag{3.4}$$

Here $u, \upsilon, w$ are the components of the speed vector along the $X, Y, Z$ axes, respectively.

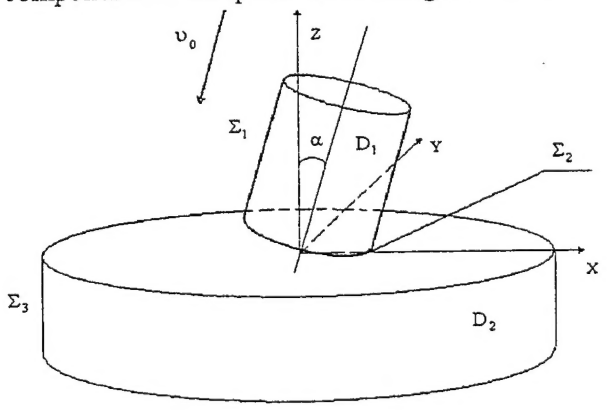


Figure 1. Statement of a problem.

The boundary conditions have the following form. The following conditions are performed at the free $\Sigma_1$, $\Sigma_3$ surfaces:

$$T_{nn} = T_{n\tau_1} = T_{n\tau_2} = 0 \text{ at } (x,y,z) \in \Sigma_1 \cup \Sigma_3, \tag{3.5}$$

at the contact surface $\Sigma_2$ the sliding conditions are realized:

$$T_{nn}^{+} = T_{nn}^{-}, T_{n\tau_1}^{+} = T_{n\tau_1}^{-} = T_{n\tau_2}^{+} = T_{n\tau_2}^{-} = 0, \upsilon_n^{+} = \upsilon_n^{-} \text{ at } (x,y,z) \in \Sigma_2. \tag{3.6}$$

Here **n** is the unit normal vector to the surface at the point under consideration, $\tau_1$ and $\tau_2$ are the interperpendicular unit vectors in the plane, tangential to the surface at this point; $T_n$ is the force vector at the surface with normal **n**; $\upsilon$ is the speed vector. The low indexes of vector $\mathbf{T_n}$ and $\upsilon$ indicates the projections onto the corresponding basis vector, the "+" sign characterizes the value of parameters in the strike, the sign "-" indicates the same in the barrier.

Thus, the equations system (2.1-2.11) fully defines the finite problem together with initial and boundary conditions (3.1-3.6).

In the framework of the preset problem the experimental and numeric investigations of interaction of steel strike with isotropic and anisotropic barrier were conducted. The numeric modeling was carried out through the method of finite elements [9-11]. The plates from isotropic glassplastic and transtropic organoplastic with an anisotropy degree $n=E_{Tx}/E_{Tz}=6.4$ were used. For considered transtropic material $E_{Tx}=E_{Ty}>E_{Tz}$. $E_I$ values for isotropic material lies in the limits of $E_{Tx}>E_I>E_{Tz}$. Here $E_{Tx}$, $E_{Ty}$, $E_{Tz}$ and $E_I$ are the modules of elasticity for the transtropic and isotropic material, respectively. Coordinate plane XOY lies in the isotropy plane of the transtropic barrier and the axis *Z* coincides with the normal to it. The compact (the diameter D is equal to length L) steel cylinders with the mass of m=10 (D=L=11.8 mm) and m=20 (D=L=14.8 mm) grams were used as the striker. In the experiments normal interaction ($\alpha = 0°$) of the strikers with barriers were provided.

Table 1 shown the results of experiments and calculations at the interaction of the striker with mass of 20 grams with the isotropic barrier. The following symbols are introduced into the table and the text: h is the barrier thickness, $\upsilon_0$ is the initial striker speed, $\upsilon_1$ is the beyond barrier speed of striker, $\varepsilon$ is the relative decrease of the striker height after barrier piercing, $\delta_\upsilon$ is the relative divergence along beyond barrier speed of striker in the experiment and calculation.

Table 1. Comparison of results of calculations and experiments

| h, mm | $\upsilon_0$, m/s | $\delta_\upsilon$, % | Experiment | | Calculation | |
|---|---|---|---|---|---|---|
| | | | $\upsilon_1$, m/s | $\varepsilon$, % | $\upsilon_1$, m/s | $\varepsilon$, % |
| 5 | 992 | 6.3 | 928 | 5.7 | 870 | 2.8 |
| 9 | 1163 | 6.2 | 1013 | 8.9 | 950 | 5.6 |
| 14 | 1064 | 4.0 | 812 | 10.4 | 780 | 9.0 |

The results on beyond barrier speeds of striker at the interaction of 20-gram striker with transtropic barrier are presented in Table 2.

The influence of anisotropy and orientation of the strength properties onto the protective barrier properties can be evaluated by the plots, presented in Figure 2. The figure shows the calculated dependencies of the resistant forces upon the time at the normal striker interaction with 10 gram transtropic and isotropic (n=1) barriers with the thickness of 24 mm. As the

calculations showed the increase in the barrier strength in XOY plane provides more substantial increase in barrier resistance to penetration (curve 3) then the increase in strength along Z (curve 2).

Table 2. Comparison of results of calculations and experiments

| h, mm | $\upsilon_0$, m/s | $\delta_\upsilon$, % | Experiment | Calculation |
|---|---|---|---|---|
| | | | $\upsilon_1$, m/s | $\upsilon_1$, m/s |
| 26 | 1054 | 8.3 | 698 | 640 |
| 26 | 1077 | 8.2 | 695 | 638 |
| 18 | 1012 | 6.8 | 897 | 836 |
| 18 | 956 | 5.5 | 838 | 792 |

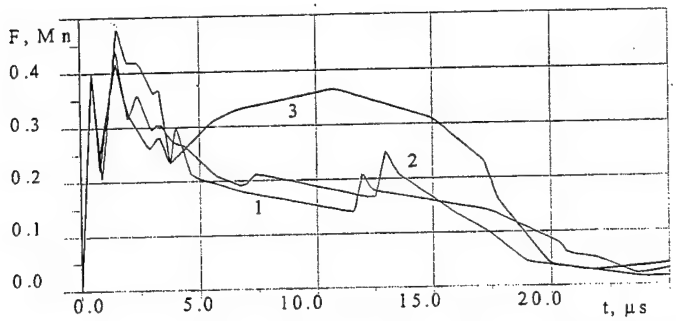


Figure 2. Resistance force vs time. $\upsilon_0$=1000 *m/s*, $\alpha$=0°, 1 – $n$=1, 2 – $n$=0.1, 3 – $n$=10.

The calculated values of beyond barrier speeds of striker with the mass 20 gram are presented in Table 3 during its interaction with the thickness of 24 mm and at different anisotropy degree (from 0.1 up to 10) at speeds of 2000 m/sec and 1000 m/sec where $\delta_{\upsilon i}$ is the relative deviation of beyond barrier speed of striker in comparison with isotropic case.

Table 3. Influence of orientation of barrier strength properties and interaction speed on beyond barrier speed of striker

| n | 0.1 | 0.3 | 1 | 6.4 | 10 |
|---|---|---|---|---|---|
| $\upsilon_0$=2000 m/s | | | | | |
| $\upsilon_1$, m/s | 1054 | 1051 | 1082 | 1060 | 1035 |
| $\delta_{\upsilon i}$, % | -2.9 | -2.9 | 0 | -2.0 | -4.0 |
| $\upsilon_0$=1000 m/s | | | | | |
| $\upsilon_1$, m/s | 533 | 557 | 578 | 468 | 371 |
| $\delta_{\upsilon i}$, % | -8.0 | -4.0 | 0 | -19.0 | -36.0 |

The analysis of the results allows to conclude that the anisotropy effect increases with the decrease of interaction speed. Various resistance of anisotropic and isotropic barriers to the penetration is due to the dynamic of destruction, being developed in them as a result of the impact. Figure 3 presents the configurations of isotropic (a) and transtropic (b) barriers with the thickness of h=19 mm, interacting with the 10 gram striker in ZOX section. The regions, in which the criterion (10) had been destructed at pressing ($e_{kk}$<0) are fully painted, and the regions

of destruction at tension ($e_{kk}>0$) are cross-hatched. The destruction of the barrier material begins in the compression wave, being initiated at the impact and developed along the barrier. The tension regions are formed as the result of reflection of compression waves from the free surfaces in the barrier. Initially they are formed at the face in the ring zone along the perimeter of the crater, being formed as the result of the reflection of compression waves from the strike side surfaces and the barrier face. Then they are formed near the end barrier surface as the result of compression wave reflection from the end surface.

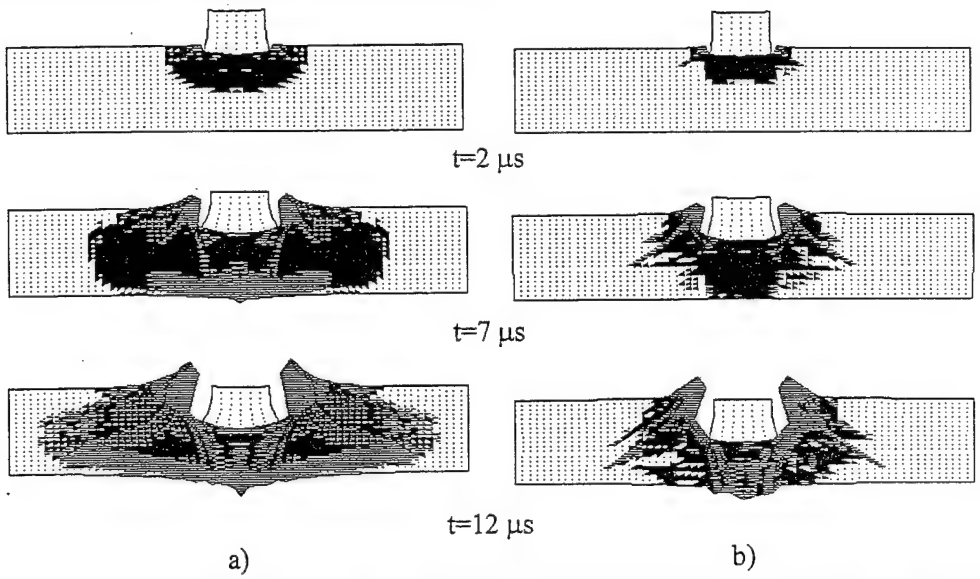


Figure 3. Evolution destruction areas in isotropic (a) and transtropic (b) barrier. $\upsilon_0$=1000 m/s, $\alpha$ =0°, h=19 mm, m=10 g.

The calculations showed that in the case under consideration the diameter of the destructed zone at the face of the transtropic barrier is 1.6 fold less then of the isotropic one and 4 fold less at the end surface (7 μs). In isotropic barrier the destruction region is extended with the propagating of the impact wave retaining vortex (initially spherical and the close to ellipsoid) form. In transtropic barrier the destruction zone in the impact wave is narrowing with its approach to the end surface. Also in transtropic barrier the narrow conic zone of destruction (crack) is separated, being propagated at the angle of 45° to Z-axis. Similar differences in the destruction character are explained by the fact that the velocity of propagation of relief waves (of sound) in transtropic barrier along X, Y and Z are various ones: $C_x=C_y>C_z$, $C_x/C_z=2.6$. Owing to this fact the relief waves, being propagated from free surfaces with the speed, greater then the impact wave one, leads to the increase in the destruction region in the compression wave in the X and *Y* direction in its interaction with the latter. The conducted experiments supported the calculation results. Figure 4 represents the photos of faces of isotropic (a) and transtropic (b) barriers after the interaction with steel strikes. The starting conditions in the experiments corresponded to the calculated ones. As it is seen from the photos, the diameter of the distracted area in the transtropic barrier is less then the one in isotropic barrier and practically coincides with the strike diameters.

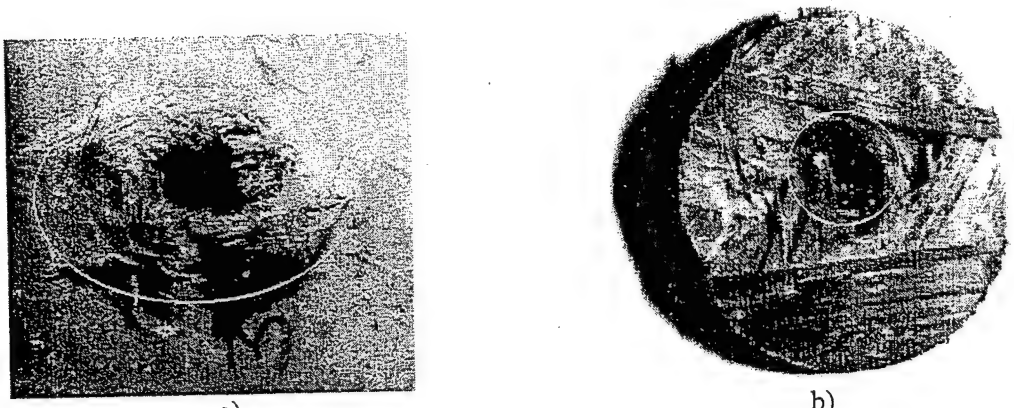

a) b)

Figure 4. Barrier faces after interaction with striker. $\upsilon_0$=1000 m/s, $\alpha$=0°, h=19 mm, m=10 g.

Further the numerical investigations of peculiarities of destruction of isotropic, transtropic and orthotropic barriers from organoplastics were carried out during interaction with 20 gram steel striker in the impact speed range of 1000 – 3000 m/sec and at the meeting angles of 0° - 60°. In the calculations the following relation of elastic material properties were provided: for transtropic material $E_{Tx}=E_{Ty}>E_{Tz}$, $n=E_{Tx}/E_{Tz}=6.8$; for orthotropic one $E_{Ox}>E_{Oy}>E_{Oz}$,$n_1=E_{Ox}/E_{Oz}=6.8$, $n_2=E_{Oy}/E_{Oz}=2.98$. For isotropic barrier the elastic characteristics had mean value $E_{Tx}>E_I>E_{Tz}$. The relation between strength parameters was provided in the same manner as for the elastic characteristics. Figure 5 shows volume configurations, illustrating the interaction process of the striker with orthotropic barrier.

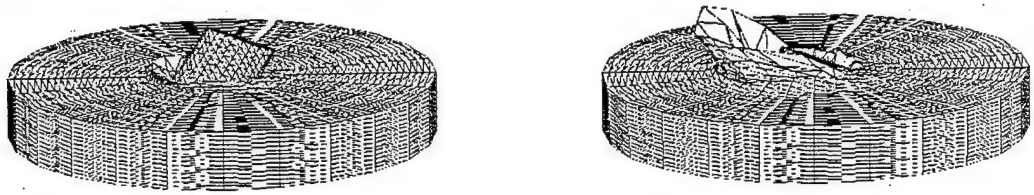

t=6 μs t=11 μs

Figure 5. Volumetric configurations of striker and orthotropic barrier. $\upsilon_0$=1500 m/s, $\alpha$ =30°, h=15 mm, m=20 g.

The results, allowing to compare the destruction in the barriers being realized to the moment of coming out of the impact wave onto the end surface are given in Table 4. The values $d_T/d_I$ and $d_O/d_I$ characterize the relation of the destructed region diameter at the face and end surface in transtropic and orthotropic plate to the corresponding diameter in the isotropic plate; $d_e/d_f$ is the relation of the destructed zone diameter at the end to the one of the face barrier surface: I – isotropic, T – transtropic, O – orthotropic.

The analysis of the investigations conducted shows that under considering conditions the diameter of the destruction region is less in anisotropic barriers (transtropic and orthotropic ones). In case the greatest increase in the destruction region is observed in orthotropic barrier: for the face the increase is 13-24 %, for the end surfaces the one is 45-63 %. Also for anisotropic barriers the greater narrowing of the destruction with the face one ($d_e/d_f$ ). Thus, if at normal ($\alpha$=0°) interaction in isotropic and transtropic barrier the narrowing is absent ($d_f=d_e$) in orthotropic one the diameter of end destruction's is 40% less then at face. In the impact at the

angle of ($\alpha$=30°, $\alpha$=60°) the narrowing for the isotropic barrier is 27-40%, for transtropic one it is 33-70%, for orthotropic: 40-72%.

Table 4. Relation of destroyed areas

| Starting conditions | Surface | $d_T/d_I$ | $d_O/d_I$ | $d_e/d_{f\,e}$ | | |
|---|---|---|---|---|---|---|
| | | | | I | T | O |
| $\upsilon_0$=1500 m/c $\alpha$ =0° | Face | 0.87 | 0.87 | 1 | 1 | 0.6 |
| | End | 0.87 | 0.53 | | | |
| $\upsilon_0$=1000 m/c $\alpha$ =30° | Face | 1 | 0.78 | 0.67 | 0.46 | 0.4 |
| | End | 0.68 | 0.47 | | | |
| $\upsilon_0$=1500 m/c $\alpha$ = 30° | Face | 0.95 | 0.76 | 0.67 | 0.64 | 0.41 |
| | End | 0.9 | 0.46 | | | |
| $\upsilon_0$=2500 m/c $\alpha$ = 30° | Face | 1 | 0.83 | 0.73 | 0.67 | 0.48 |
| | End | 0.91 | 0.55 | | | |
| $\upsilon_0$=1500 m/c $\alpha$ = 60° | Face | 1 | 0.78 | 0.6 | 0.3 | 0.28 |
| | End | 0.5 | 0.37 | | | |

Figures 6-8 illustrate (ZOX in section) the destruction dynamics of isotropic (Figure 6), transtropic (Figure 7) and orthotropic (Figure 8) barriers at normal interaction with the striker. Figure 9 shows at the same time configurations of isotropic (a), transtropic (b), and orthotropic (c) barriers at the interaction of the striker at the angle of $\alpha = 30°$. The indication of the destruction region is similar to Figure 3.

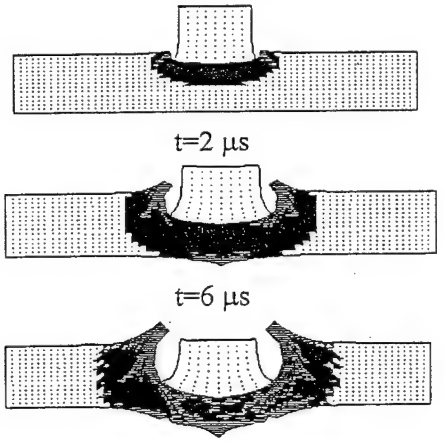


Figure 6. Destruction areas evolution in isotropic barrier. $\upsilon_0$=1500 m/s, $\alpha$=0°, h=15 mm, m=20 g.

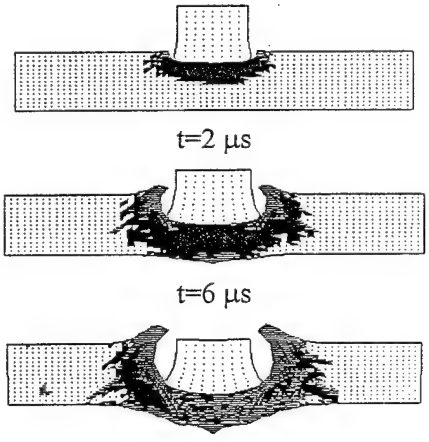


Figure 7. Destruction areas evolution in transtropic barrier. $\upsilon_0$=1500 m/s, $\alpha$=0°, h=15 mm, m=20 g.

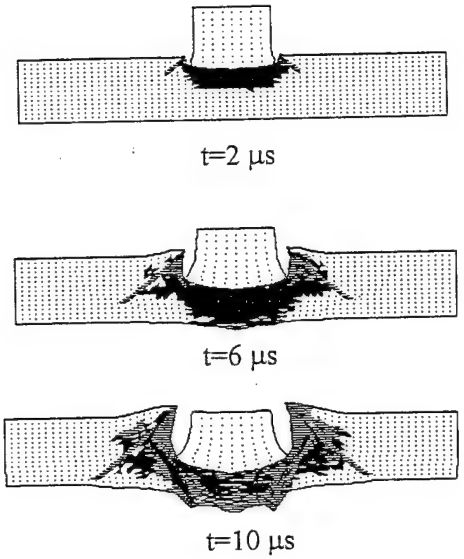


Figure 8. Destruction areas evolution in orthotropic barrier. $\upsilon_0$=1500 m/s, $\alpha$=0°, h=15 mm, m=20 g.

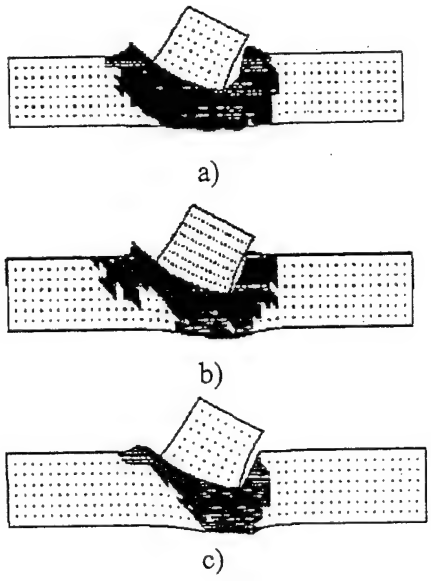


Figure 9. Comparison of destruction areas. $\upsilon_0$=1000 m/s, $\alpha$=30°, h=15 mm, t=11 μs, m=20 g.

### 3.2 Evolution of compression waves in the anisotropic material

Coordinated experimental and numerical investigations on evolution of compression wave in isotropic and anisotropic materials were conducted [23]. The method of recording of pressure profiles with filled-system transducers is one of the most justified and widely spread experimental methods of dynamic test of materials [12]. The device, (Figure 10) designed for generation of one-dimension waves and recording of pressure profiles with manganine transducers in the materials, being tested [13], was used in realization of experimental investigations.

Main parts of the device are: powder gun with gauge of 50mm, striker, mantle ring with units of contact transducers for recording of striker's speed and synchronization of with IBM PC for automized treatment of experimental results. The samples are two plane-parallel plates, being mechanically fixed, (plate-screen and stop plate), manganine pressure transducers is placed between the plates. In the transducers the manganite foil with the thickness of 0.03mm was used: it metrologic characteristics are reliably fixed for recording of tension on waves [12]. Combined strikers (Figure 11) which were represented as cylinders with length of 50mm from textolite, the steel plate with the diameters of 46 and variable thickness from 3 up to 7mm being pressed into them, were used for dynamic loading of samples and generation of plane impact waves. It allowed to vary the duration of impact pulse. Strikers were bring up to speed in the range of 100-800m/sec.

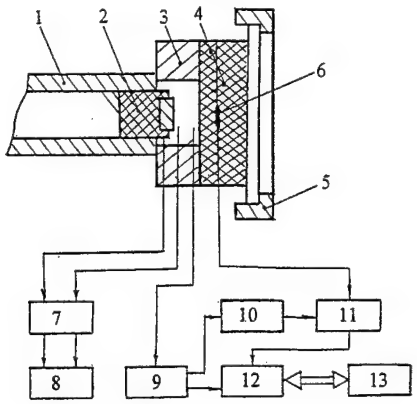


Figure 10. The scheme of the experimental complex for pressure recording in materials in impact testing. 1 - powder gun, 2 - striker, 3 - stop ring with the unit of contact transducers, 4 - sample under investigation, 5 - tighten upring, 6 - manganine transducer, 7 - unit for pulse formation, 8 - numeric frequency meter, 9 - synchronization unit, 10 - pulse power unit of manganine transducer, 11 - Witstone bridge, 12 - digit two-channel oscilograph, 13 - IBM PC.

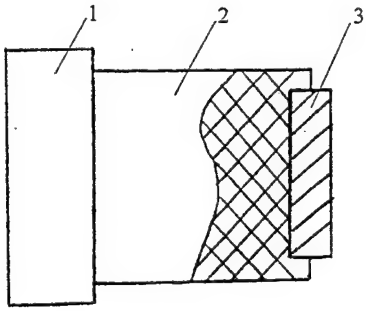


Figure 11. 1 - mantle ring, 2 - tray, 3 - metal striker.

Plane compression wave has been formed in screen plate and the striker as a result of impact. The speed of compression wave propagation in the screen was determined by two manganine pressure transducers, being located on the sample surface. The thickness of strikers and screen plates was selected in such a manners, that relief waves from free surfaces wouldn't distort the pattern of one-dimension deformation in compression wave. A number of experiments were conducted according to the forementioned_method and oscillograth records of pressure change in time for isotropic (Figure 12a) and anisotropic materials (Figure 12b, Figure 12c) were obtained under different starting conditions. KAST-B glass textolite, the material with well studied characteristics [14] was used as the standard material. Experimental conditions were simulated numerically on the base of the model [3-8]. The experimental and calculated profile of tension in anisotropic material is presented in Figure 12d.

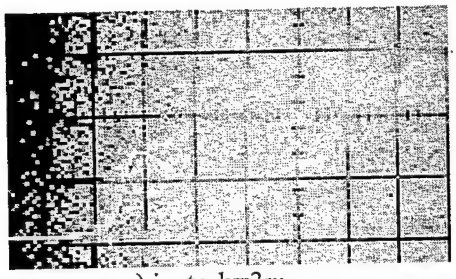

a) isotr. h=3*m*

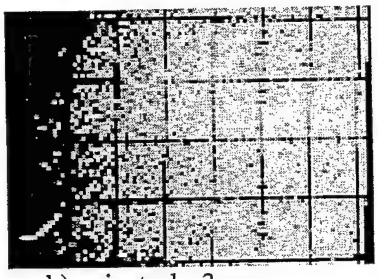

b) anisotr. h=3*mm*

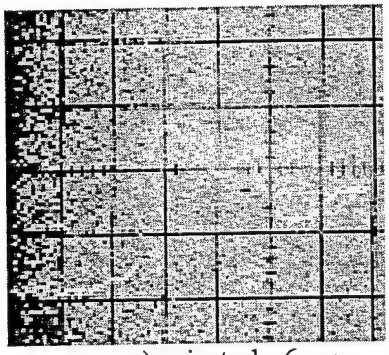

c) anisotr. h=6*mm*

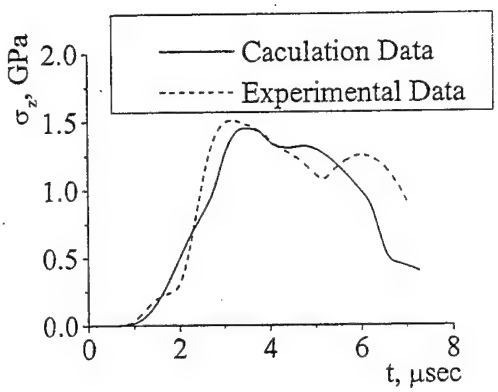


d) anisotr. h=6*mm*

Figure 12. $\upsilon_0$=490 *m/s*

### 3.3 Influence of orientation elastic and strength properties on destruction and evolution of wave processes in the orthotropic material

Let's consider the interaction of steel isotropic compact and elongated strikers with orthotropic plate. Impact interaction occurs in velocity range of $\upsilon_0$=700-2000 m/sec and at the angle of meeting of $\alpha$=0-75°. The method of finite elements is used for the solution [9-11]. The starting material (material 1) of the plate has following mechanical properties' relations: $E_x>E_y>E_z$, $E_x/E_y=2.28$, $E_x/E_z=6.8$, $\sigma_{bx}>\sigma_{by}>\sigma_{bz}$, $\sigma_{bx}/\sigma_{by}=2.26$, $\sigma_{bx}/\sigma_{bz}=6.8$, where $E_x$, $E_y$, $E_z$ a modulus of elasticity, $\sigma_{bx}$, $\sigma_{by}$, $\sigma_{bz}$ are ultimate strength in correspondent directions from [3-8, 15, 17]. Material 2 we will obtain from the initial one through the turn of its properties about OY axis of 90°, assuming that for anisotropic material under consideration there exists the elastic potential and the relation $E_k\nu_{ik}=E_i\nu_{ki}=$, $\nu_{ki}$ are Poisson's ratios, i, k=x, y, z. Then for the material 2 we will obtain following relation of characteristics in the starting system of coordinates: $E_x<E_y<E_z$, $E_x/E_y=0.34$, $E_x/E_z=0.15$, $\sigma_{bx}<\sigma_{by}<\sigma_{bz}$, $\sigma_{bx}/\sigma_{by}=0.33$, $\sigma_{bx}/\sigma_{bz}=0.15$. Figure 13 shows calculated configurations of compact striker and plates, made out of material 1 and 2 in ZOX cross-section at various moments under normal interaction ($\alpha$=0°). Areas, in which the material of plate fails at $e_{kk}\leq 0$ are colored fully, and the ones, where failure occurs at $e_{kk}> 0$ are dashed. The failure of the plate material begins in compression wave, being initiated at the

moment of impact. In the material 1 the failure, proceeding in compression wave propagates through total plate thickness. In the material 2, the failure in compression wave takes place only in the upper part of the plate, but the width of this area in ZOX cross-section is 1.4-1.7 fold higher (in dependence on impact velocity) then the corresponding one in material 1. Such distinctions are explained not only by the variety in strength parameters, but various velocities $c_i$ of propagation of waves in material 1 and 2 in corresponding directions: i=x, y, z.

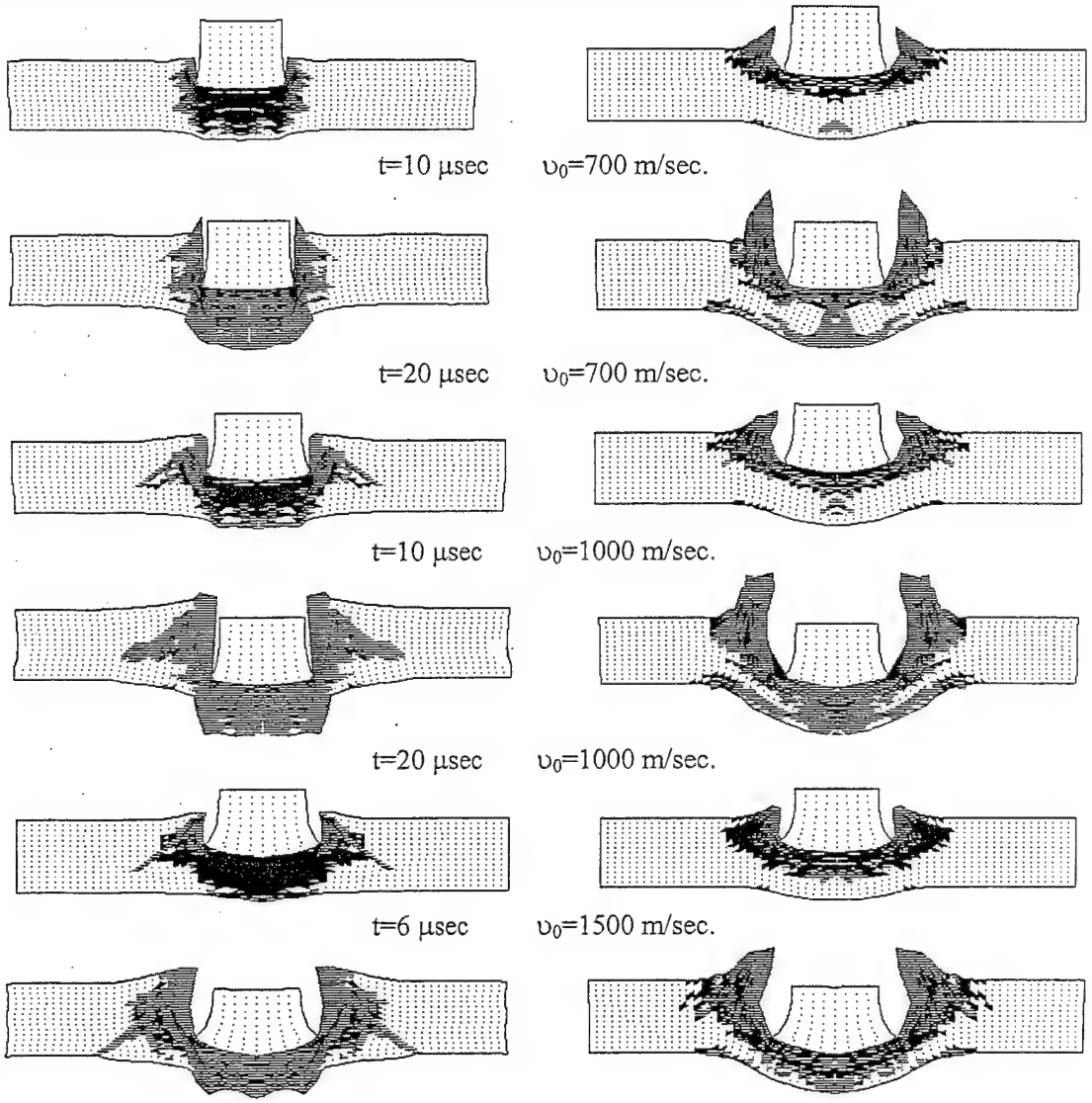


Figure 13. Material 1 is to the left, material 2 is to the right.

In the material 1 $c_x/c_z=2.61$ it lead to the fact that relief waves, propagating from the side surface of the striker and plate surface decreases (to the lager extent) the width of compression wave front in material 1 then in material 2, where $c_x<c_z$. The development of narrow zone of failure (crack), propagating from plate surface at the angle of 45° to OZ axis, is characteristic

feature for material 1 with the increase in impact velocity. At impact velocities up to 1000 m/sec this zone doesn't come on to back surface of the plate. The crack reaches the back surface with the increase in interaction velocity. In the material 2, due to the fact that $c_x<c_z$, relief waves have greater velocity component in z direction and, on overtaking the compression wave, decrease the degree of compression stress. Further propagation of weakened compression wave hasn't already cause the failure in the material.

In more details the proceeding of wave processes in materials may be traced according to plots of distribution of stress component $\sigma_z$ in the plate along through thickness along Z-axis at different time moments (Figure 14a – Figure 14c). On plots the point with coordinate z=0 correspond to back surface of plate. To 1.5 μsec (Figure 14a) in z direction the front of compression wave in material 2 propagating over 2/3 of plate thickness an in material 1 over 1/3 of plate thickness. At the same time in material 2 relief wave being formed on side surface of striker and face of the plate portion of curve 2 on segment with coordinates $z_1$=14 mm and $z_2$=13 mm begins to overtake compression wave.

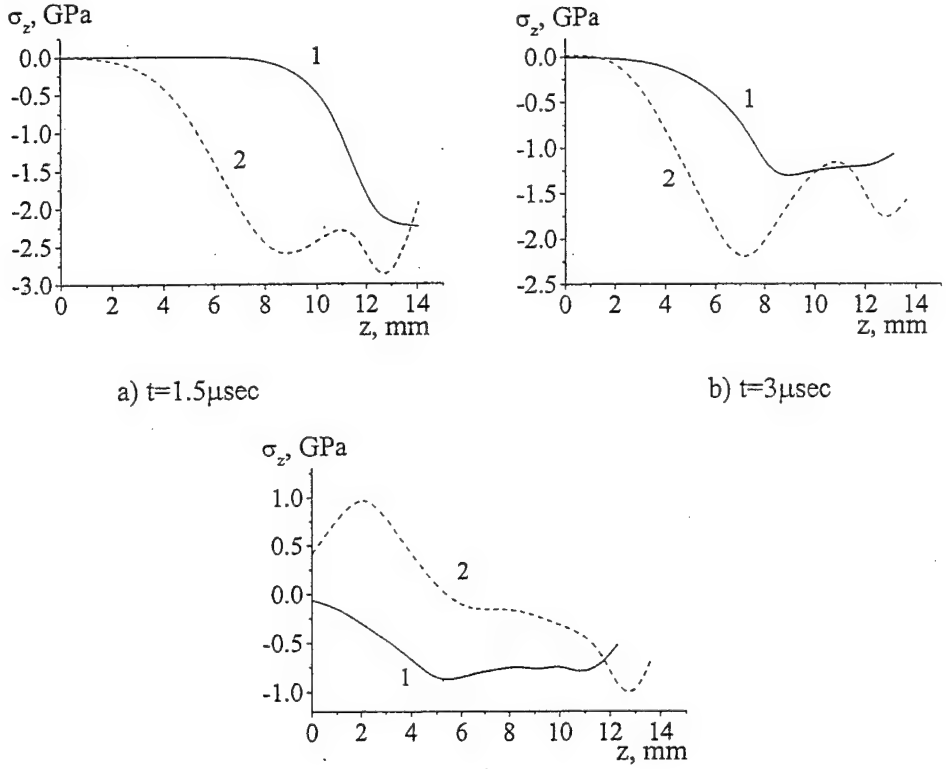


Figure 14. Distribution $\sigma_z$. $\upsilon_0$=700 m/sec. 1 – material 1, 2 – material 2.

Figure 14c characterizes stressed state in materials, established after passage of compression wave. To this moment of time compression wave in material 1 reaches back surface and through material the relief wave is already propagating which was formed as a result of reflection of

compression wave from back surface of plate. The level of compressive stresses in material 2, retained in upper half of plate is substantially less (2 - 3 - fold) then in material 1.

In 3 μsec after impact (Figure 14b) relief wave substantially weakens compression wave in material 2 – maximum value of strain in it in comparison with 1.5 μsec decreases from 3 GPa up to 2.2 GPa. To this moment of time region in materials 1 and 2 behind the front of compression waves (9 mm < z < 14 mm) are failured ones. Further propagation of compression wave in material 2 doesn't result in failure. On the contrary in material 1 failure in compression wave takes place over total thickness of plate.

Approximately the same level of compressive stresses retains only near contact surface of the striker and the plate. The area of maximum tension stresses, in which failure takes place (Figure 13) forms in material 2 in section with coordinate z = 2 mm as a result of interference of relief waves. Thus, relief wave, reflected from back surface, in material 1 propagates though weakened, failured by compression wave material, which has compressive strength only. That results in complete failure of the material placed before introducing striker, practically trough total thickness of plate. Inmaterial 2, reflected relief wave propagates through unfailured material, causing the distractions of chipping off character near back surface of plate. Further development of failure in material 2 is not to wave processed but occur as a result of development of tensile stresses on introduction of striker.

The plots on Figure 15 allow to evaluate the portion of the material, being failured completely in the plate, and showing no failure resistance. During the whole process of the striker interaction with plates, the portion of complete failures in the material 1, exceeds the corresponding values in material 2. The values of residual striker's velocity after punching of plates also speaks about the fact that material 2 has greater resistance to impact failure and permeability – for all starting velocities under consideration, more intense retardation of the striker is observed on its interaction with the plate made out of material 2. The difference in striker velocity after punching of plates, made out of material 1 and 2 increases with decrease in interaction velocity: for $\upsilon_0$=1500 m/sec it is 5%, for $\upsilon_0$=1000 m/sec – 12%, for $\upsilon_0$=700 m/sec – 20%.

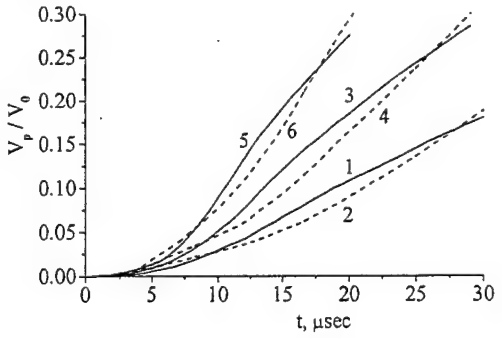


Figure 15. The change in time of relative amount of the material, being failured at $e_{kk}$>0. 1, 3, 5 – in material 1; 2, 4, 6 – in material 2 at $\upsilon_0$=700 m/sec, 1000 m/sec, and 1500 m/sec, respectively.

The volumetric configurations showing process of interaction elongated striker with a plate from the material 1 at angle are given on Figure 16.

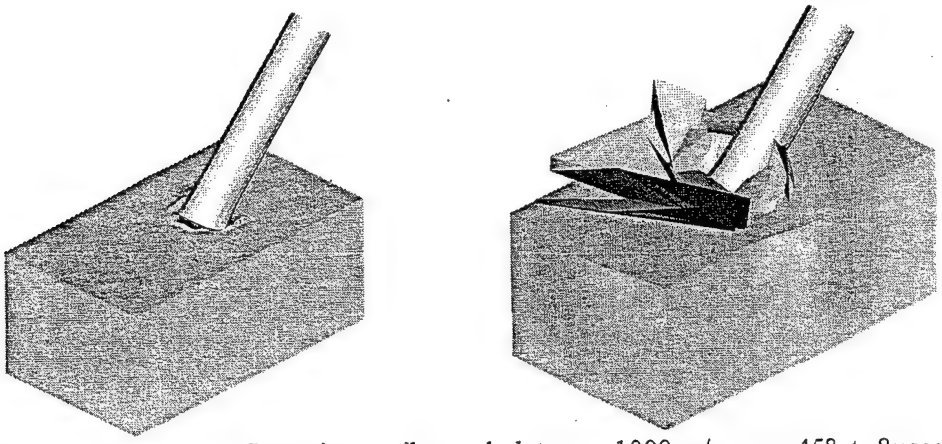

Figure 16. Volumetric configurations striker and plate. $\upsilon_0$=1000 m/sec, $\alpha$=45°. t=8μsec - at the left, t=24μsec - on the right.

Figure 17 and 18 show volume and in ZOX cross-section configurations of elongated steel striker, interacting with the plate, made from the material 1 (Figure 17) and the material 2 (Figure 18) at the angle $\alpha$=45°. As a whole, the qualitative picture of development of destructions and courses of wave processes in materials 1 and 2, in this case is similar to the case of normal impact. But in too time are available a number of essential distinctions which can be looked after on Figure 19 where are given isolines $\sigma_z$. As well as at normal impact the compression wave in the material 2 reaches the back surface of a plate much earlier and is reflected from it by the relief wave. But in this case, by virtue of geometrical conditions of interaction, its front considerably already also lowers the level of stress only in the central part of the compression wave. It is illustrated by concavity isolines $\sigma_z$ in the material 2.

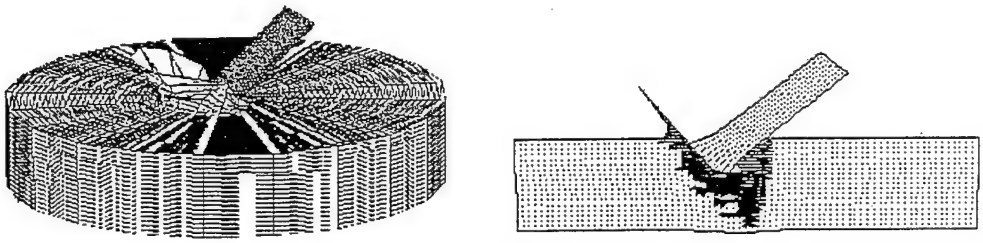

t=20 μsec

Figure 17. Material of plate - material 1, $\upsilon_0$=1000 m/sec

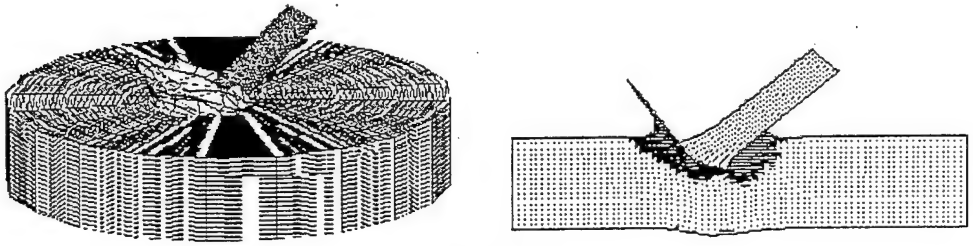

t=20 μsec

Figure 18. Material of plate - material 2, $\upsilon_0$=1000 m/sec

The analysis of change in time striker speed at interaction at angle as well as at normal impact, shows, that in a direction z the braking of striker occurs more intensively at its interaction to a plate from the material 2. So to 30 μsec the difference in speed is 6 %.

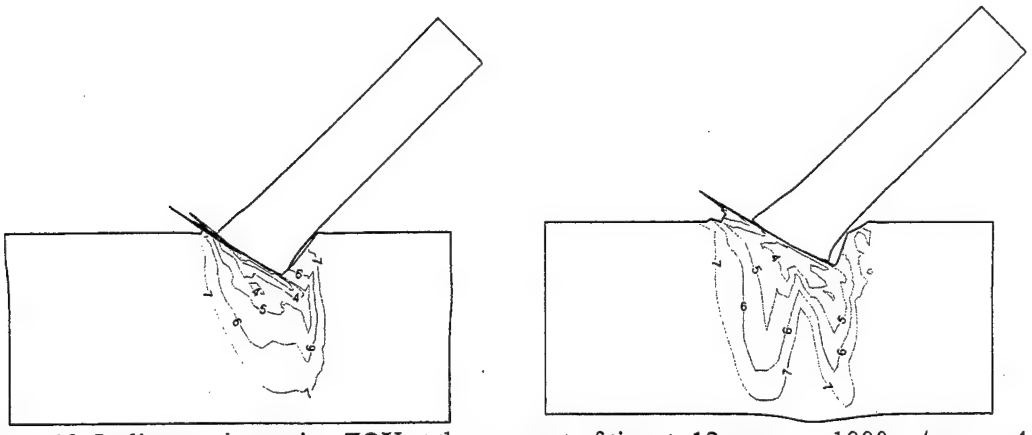

Figure 19. Isolines $\sigma_z$ in section ZOX at the moment of time t=12μsec. $\upsilon_0$=1000 m/sec, $\alpha$=45°, where 1 –2GPa, 2 --1.7 _., 7 - 0.2GPa. The material 1 - at the left, a material 2 - on the right.

### 3.4 Numerical simulation of impact loading of solid fuel fastened with orthotropic shell

One of the main problems of the operational safety of solid fuel rocket engines (SFRE) is the prediction of their behaviour under loads of various types. At certain levels of external actions, conditions sufficient for detonation initiation may be created in the solid fuel. The reliability and safety of SFRE may be increased owing to the increase in construction effectivity of the shell material. If the direction of load action is known beforehand, one of the popular methods of increasing of operation characteristics is the orientation of properties, i.e. the transfer of the degree of order to the structure, the other method is the reinforcement of the material with strengthening elements. The behaviour of such anisotropic materials under deformation substantially differs from the one of isotropic materials: the spheric body, subjected to overall compression, transforms to ellipsoid, the bending of anisotropic beam is followed by twisting. Rates of propagation of stress waves in anisotropic materials depend on the direction of wave propagation, and also on level of stresses beyond elasticity limit. For example in anisotropic materials, in several directions, the transverse wave appears to be faster and the longitudinal one to be slower. Owing to this fact, the picture of interaction of reflected waves in anisotropic materials changes substantially. Since, at pulse exposure on the material, the area, in which the energy is concentrated, is limited by rates of distribution of waves; it is possible to change directionally the distribution of stress waves nearby the zone of pulse loading, through the change of the anisotropy degree of the of the material. This fact is most important in problems, in which shock-wave phenomena play the determining role in initiation of transition processes (e.g. detonation).

Normal interaction of single steel cylinder strikers and oblique impact, both simultaneous and at different times of multiple, converging steel spheric particles with SFRE are considered in the work. The shell material is orthotropic organoplastic, the behaviour of which is described according to [16, 20, 22]. Elastic media simulates the behaviour of solid fuel. The range of impact velocities from 400 up to 2000m/sec is investigated. It should be noted that this range of

impact velocities is one of the most dangerous for SFRE and aircrafts since thin protection screens are ineffective in this case especially against sufficiently hard particles.

The behaviour of steel strikers is described by elastic-plastic medium with the yield strength equal to 1Gpa [1, 6]. Components of stress tensor in the shell materials are determined from relations for orthotropic material (2.8). For the description of the shell failure the tensor-polynomial criterion of the strength of the forth degree is used (Equation (2.10)). The behaviour of the fuel is described by elastic medium in which the modulus of elasticity depends on pressure E=f(P). The mean stress (pressure) is calculated according to the formula [19]

$$P = \left[ \exp\left( 4\beta \frac{V_0 - V}{V_0} \right) - 1 \right] \frac{\rho_0 \alpha^2}{4\beta} \qquad (3.7)$$

Where $\rho_0$ is the starting density, $\alpha$ and $\beta$ are coefficients of impact adiabat $D = \alpha + \beta u_m$, $u_m$ is mass velocity, $V_0$ and V are the starting and current specific volumes.

*3.4.1 Single impact*

Let's consider the normal impact of a steel cylinder striker with SFRE element, which is the two-layer barrier (Figure 20). The striker occupies $D_1$ area, the shell occupies $D_2$ the fuel occupies $D_3$ area. The axis Z coincides with the one of the striker and is directed on to the side, being opposite to the impact direction.

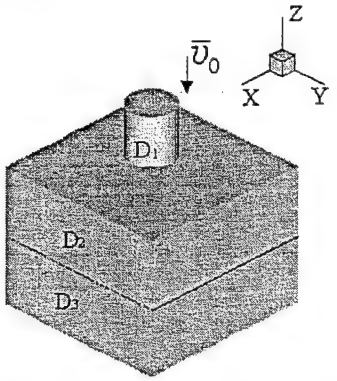


Figure 20. Statement of the problem of single impact.

Symmetry axes of orthotropic shell material coincides with axes of coordinate system. The problem with starting (t=0), boundary conditions is set for Equation(2.1) - Equation (2.11).
Starting conditions (t=0)

$$\sigma_{ij} = E = u = v = w = 0 \text{ at } (x,y,z) \in D_2 \cup D_3, i,j = x,y,z$$

$$\sigma_{ij} = E = u = v = 0, w = \upsilon_0 \text{ at } (x,y,z) \in D_1 \qquad (3.8)$$

$$\rho_0 = \rho_{0i} \text{ at } (x,y,z) \in D_i, i = 1,2,3$$

Boundary conditions are as follows: on free surfaces conditions are fulfilled:

$$T_{nn} = T_{n\tau_1} = T_{n\tau_2} = 0 \qquad (3.9)$$

on contact surface between the striker and the shell conditions of sliding without friction are realized:

$$T_{nn}^{+} = T_{nn}^{-}, T_{n\tau_1}^{+} = T_{n\tau_1}^{-} = T_{n\tau_2}^{+} = T_{n\tau_2}^{-} = 0, \upsilon_n^{+} = \upsilon_n^{-} \qquad (3.10)$$

on contact surface between the shell and the fuel adhesion condition are fulfilled:

$$u^{+} = u^{-},\ v^{+} = v^{-},\ w^{+} = w^{-} \qquad (3.11)$$

Here n is the unit vector normal to the plane under consideration, $\tau_1$ and $\tau_2$ are the perpendicular unit vectors in the plane, tangent to the surface at this point, $T_n$ is the vector of force on the site with n normal, $\upsilon$ is speed vector. Low indexed in vectors $T_n$ and n denotes the projections on to corresponding vectors of basis, sign "+" characterizes the value of parameters in the material up from the boundary, the sing "-" means down from it.

Evaluation of operational safety of SFRE, experiencing intense loads requires knowledge of the dynamics of the strain-stress state. This will allow definition of boundaries of safe external actions and to specify requirements for the shell material. On striker impact the initiation of detonation in the fuel is possible owing to two factors: 1) due to the action of shock-wave, being initiated on interaction of the striker with the shell, on the fuel, 2) due to the penetration of the striker into the fuel after failure of shell layer. Here we will consider strain-stress state, being realized in fuel at the first stage - on shock-wave outlet on it and influence of shell material properties on strain-stress state. Loading of the two-layer construction was effected with various types of steel cylinder strikers. Compact strikers (diameter $d_0$ is equal length $l_0$), 10g and 20g mass, $d_0=l_0=11.5$mm and $d_0=l_0=15$mm, with velocities $\upsilon_0=2000$m/sec and $\upsilon_0=1000$m/sec, respectively. And the striker 660g in mass, of dimensions $d_0=60$mm, $l_0=28$mm with velocity $\upsilon_0=400$m/sec. Shell thickness $H_0$ is 18mm. Poisson's ratio of the fuel under consideration was $\nu=0.495$, the relationship of densities of shell material, $\rho_1$, and fuel, $\rho_1$, is $\rho_1/\rho_2=1.4$. Let's consider two cases of properties orientation of orthotropic material of shell. The starting material (material 1) of the shell has following relations of mechanical properties: $E_x > E_y > E_z$, $E_x/E_y = 2.28$, $E_x/E_y = 2.28$, $\sigma_{bx} > \sigma_{by} > \sigma_{bz}$, $\sigma_{bx}/\sigma_{by} = 2.26$, $\sigma_{bx}/\sigma_{bz} = 6.8$, where $E_x, E_y, E_z$ are modulus of elasticity ($E_x$=48.6GPa), $\sigma_{bx}, \sigma_{by}, \sigma_{bz}$ are ultimate strength ($\sigma_{bx}$=2.67GPa) in corresponding directions from (5). Material 2 was obtained from the starting one through the rotation of its properties about the axis OY through $90^0$ (A.V. Radchenko et al., 1999), assuming, that for anisotropic material under consideration there exists elastic potential and, consequently, relations $E_k\nu_{ik} = E_i\nu_{ki}$ are fulfilled, where $\nu_{ki}$ are Poisson's ratios, i,k=x,y,z.. Then, for material 2 we will obtain following relation of characteristics in the starting coordinate system: $E_x < E_y < E_z$, $E_x/E_y = 0.34$, $E_x/E_y = 0.15$, $\sigma_{bx} < \sigma_{by} < \sigma_{bz}$, $\sigma_{bx}/\sigma_{by} = 0.33$, $\sigma_{bx}/\sigma_{bz} = 0.15$, $E_x$=7.14GPa, $\sigma_{bx}$=0.39GPa. In Figure 21 configurations of the striker of mass 660g, SFRE elements and pressure isoline are illustrated in cross section ZOX for cases when the shell is made from material 1 (a) and material 2 (b). In the material 2, the velocity of sound wave propagation in the direction z is higher, then in direction x ($c_z/c_x = 2.61$, $c_z$=6000m/sec), that

leads to the fact, that shock-wave, reaches the boundary, "shell-fuel" well before, then in material 1.

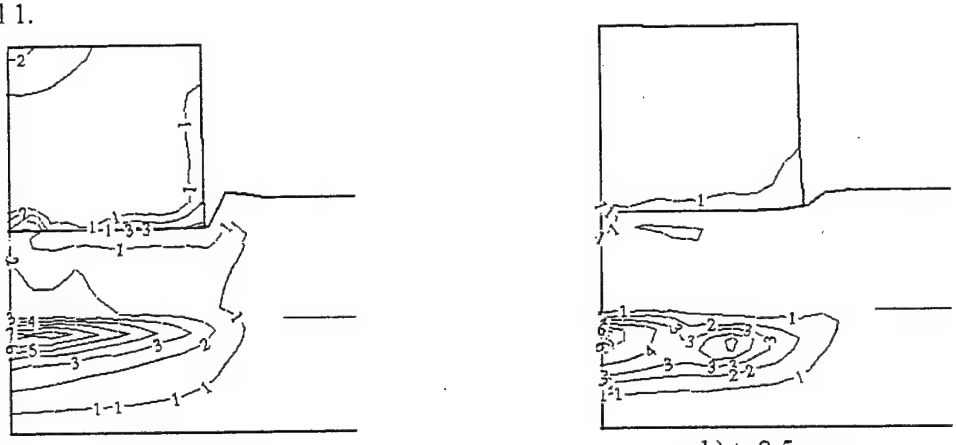

a) t=12.5μsec b) t=8.5μsec

Figure 21. Distribution of pressure isolines. $\upsilon_0$=400m/sec. a) 1 - 0.2, 2 - 0.6, 3 - 1,..., 9 - 3.4GPa; b) 1 - 0.5, 2 - 1.5, 3 - 2.5,..., 8 - 7.5GPa.

Level of pressures; being realized in the fuel, is more then 2 times less than for the material 2, when material 1 is used as shell material. Such effect is reached owing to anisotropy of shell material properties. In material 1 $c_x > c_z$ that leads to the fact relief waves, propagating from side surface of the striker and the face of the shell, have managed to reach the shock-wave front and attenuated it. On the contrary in the material 2 $c_x < c_z$ and side waves of relief have no influence on shock-wave. Dynamics of measurement in time of stressed state in the fuel at "shell-fuel" interface lying on axis OZ can be followed according to curves showed in Figure 22. Curve 1 corresponds to the case when material of the shell is material 1, curve 2 corresponds to the case when material 2 is the shell material.

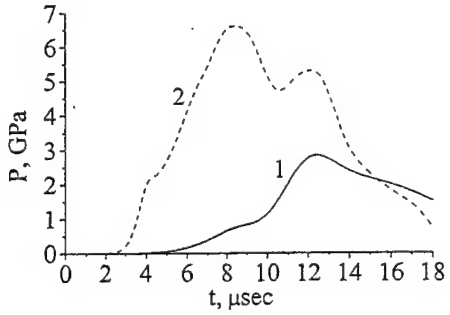


Figure 22. Changes in times of the pressure.

The configuration of the striker 20g in mass and SFRE element with the distribution of pressure isolines for two cases of orientation of shell material properties (analogues to Figure 21) are shown in Figure 23. Plots of pressure changes in time, corresponding to the case (analogues to Figure 22) are illustrated in Figure 24.

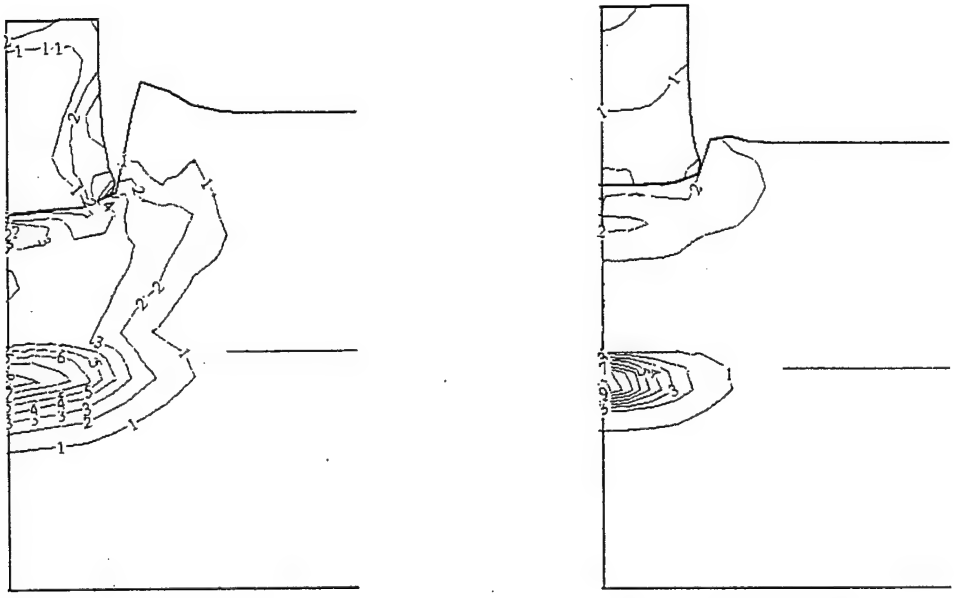

a) t=8.5μsec b) t=4μsec

Figure 23. Distribution of pressure isolines. $\upsilon_0$=1000m/sec. a) 1 - 0.2, 2 - 0.4, ..., 8 - 1.6GPa; b) 1 - 0.2, 2 - 1.2, 3 - 2.2,...,9 - 8.2GPa.

The picture of stressed state in SFRE for "heavy" and "light" strikers is qualitatively similar. But despite the fact that the velocity of "light" striker is 2.5 times higher, the level of maximum pressures, being achieved in the fuel moderately differs from the case of impact with "heavy" striker.

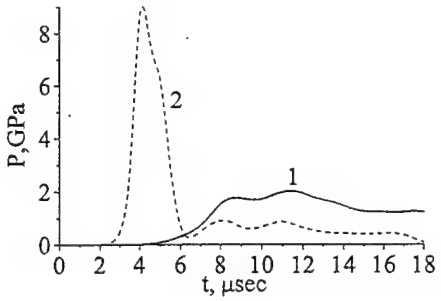


Figure 24. Changes in times of the pressure.

It is explained by the relation of geometrical parameters of strikes and the shell. Owing to the fact that the length of "heavy" striker is almost 2 times more that the "light" one the relief wave, arising on its back surface, doesn't manage to reach the shock-wave front during its passage through the shell thickness. In the case with the "light" striker, the relief wave from back surface manages to attenuate the chock wave before the moment of its outlet to the fuel. The evaluation of possibility of detonation initialization in the fuel was determinate of critical pressure $P^*$ and critical diameter $d^*$. It is supposed that the detonation arises, if are fulfilled conditions $P \geq P^*$ and $d \geq d^*$, where d - diameter, on which the values of pressures exceeding

critical value $P^*$ are reached. For the fuel type under consideration, conditions of detonation initialization arise when material 2 is used as shell material. In this case the values of pressures and diameters exceed critical ones for all types of strikes under consideration.

Thus, two factors provide the attenuation of shock-wave in material 1: side relief waves and the relief wave from the back surface of the striker; in material 2 the attenuation of the shock-wave is possible only due to back surface relief wave. That is, the selection of the material 1 as shell material is optimum one from the point of view of operational safety.

### *3.4.2 Impact by Multiple Strikers*

Let's consider the interaction of four steel spherical particles 8mm in diameter with SFRE element. The geometry of impact is illustrated in Figure 25.

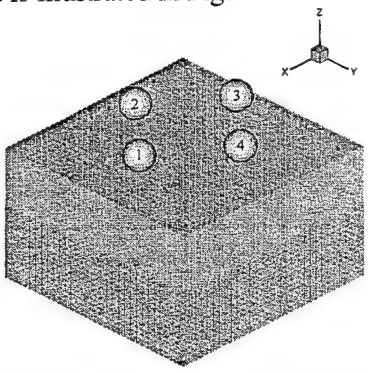


Figure 25. The geometry of interaction of particles with two layer barrier.

Impact velocity of the particles is 2000m/sec. The velocity vector of each particle is directed at an angle of $45^0$ to the plane XOY. The movement of particles is a converged one and directed to the centre of the barrier, the upper layer of which is orthotropic organoplastic and the lower one is solid fuel. Particle trajectories intersect with a shell at a distance of 15mm from central point (x=y=0). Simultaneous and different impact times are investigated for two cases of properties orientation of the shell material (material 1 and material 2). For the non-simultaneous impacts particle 1 is the first one which comes into interaction with the barrier (at time moment t=0) and then particles 2, 3 and 4 with the interval of 1μsec. All possible interactions between particles are taken into consideration in calculations. On contact surface between particles and the shell, the conditions of sliding are realized Equation(3.10), on contact surface between the shell and the fuel adhesion conditions Equation (3.11) are fulfilled. In this case the thickness of the shell was 15mm. Volume configurations of particles and SFRE element, illustrating the process of the interaction, for the non-simultaneous impacts, are shown in Figure 26. Configurations of interacting bodies with the distribution of pressure isoline in ZX (a) and ZY (b) cross sections on simultaneous and for the non-simultaneous impacts for the two types of shell material are shown in Figure 27 - Figure 30.

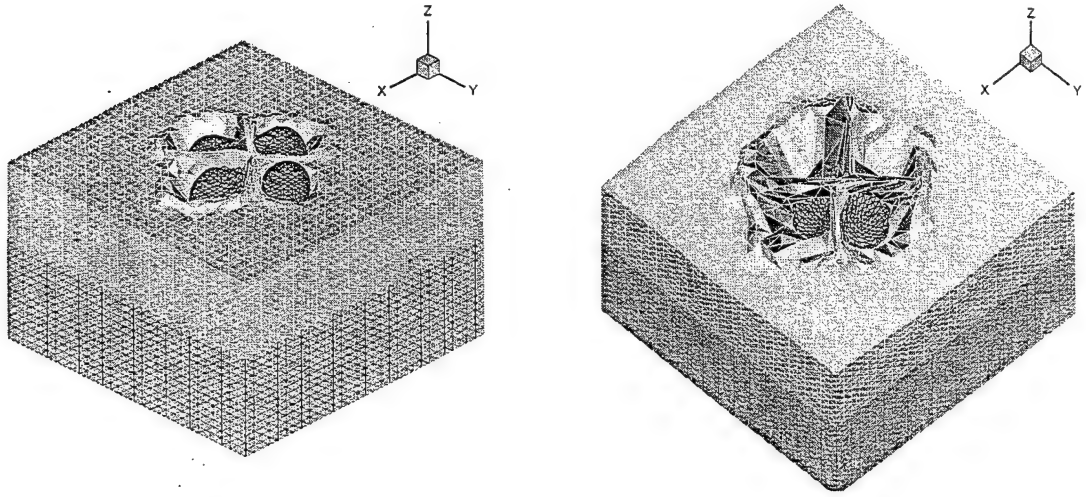


t=6μsec t=10μsec

Figure 26. Volume configurations of interacting bodies. Material 2 is the shell material.

The analysis of strain-stress state shows that for simultaneous impact, four regions of high pressure are formed in the fuel; they are formed as a result of coming out of impact waves from each of the particle. In this case regions are combining into one region, as time passes, maximum pressures in this region shift to the centre with introduction of particles.

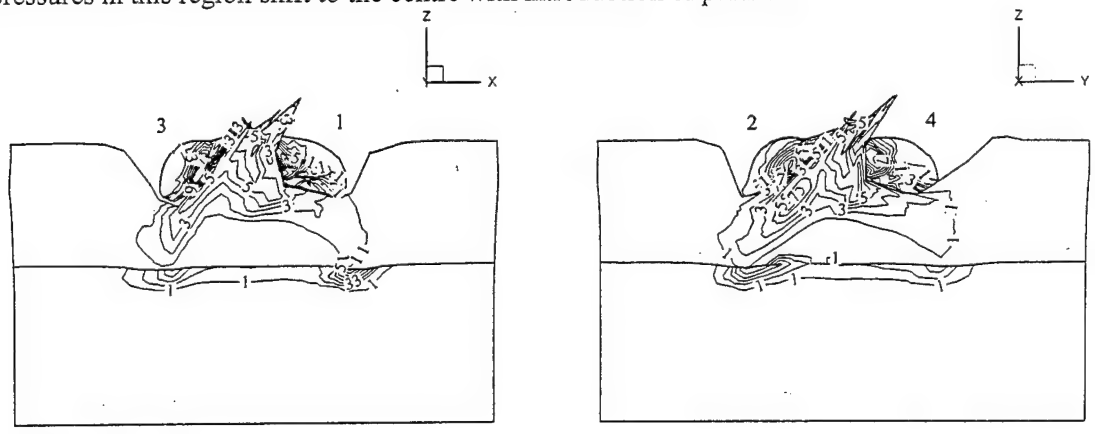


a) b)

Figure 27. Distribution of pressure isolines in cross sections ZX (a) and ZY (b) on simultaneous impact. Material 1 is the shell material. t=6μsec.1 - 1GPa, 2 - 2GPa, ...,10 - 10GPa.

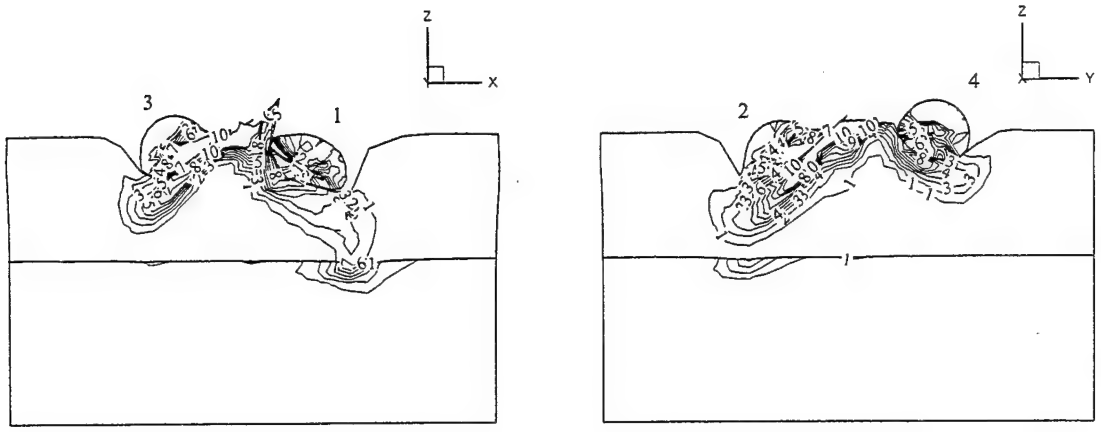


a) b)

Figure 28. Distribution of pressure isolines in cross sections ZX (a) and ZY (b) on different in time impact. Material 1 is the shell material. t=6μsec. 1 - 1GPa, 2 - 1.5GPa, …,10 - 5GPa.

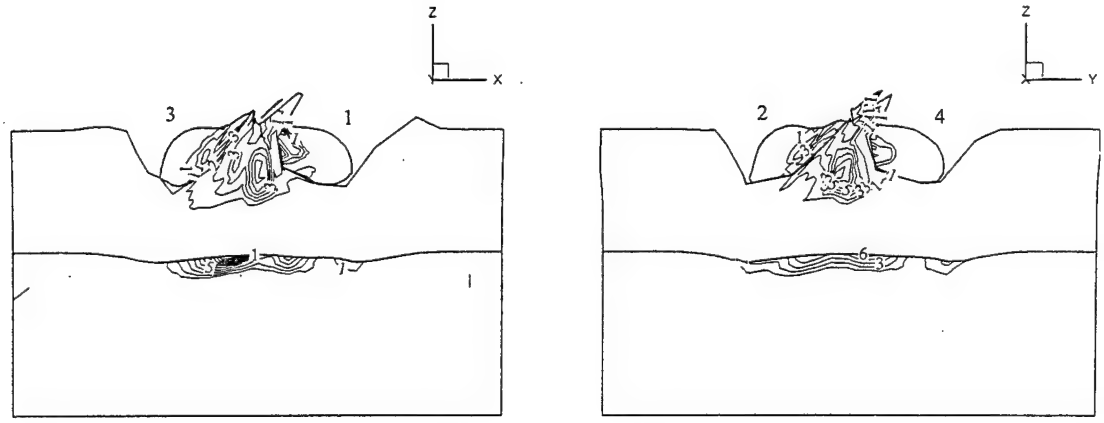


a) b)

Figure 29. Distribution of pressure isolines in cross sections *ZX* (a) and *ZY* (b) on simultaneous impact. Material 2 is the shell material. t=6μsec. 1 - 4GPa, 2 - 6GPa, 3 - 8GPa,…,10 - 22GPa.

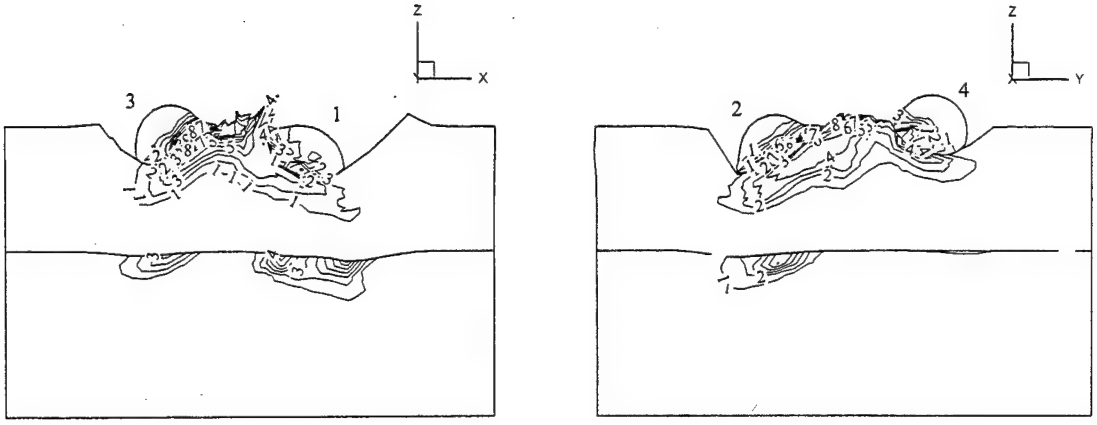


a) b)

Figure 30. Distribution of pressure isolines in cross sections ZX (a) and ZY (b) on different in time impact.Material 2 is the shell material. t=6μsec. 1 - 1GPa, 2 - 2GPa, ..., 10 - 10GPa.

For the non-simultaneous impacts the picture becomes more complex. In this case the effect of orientation of properties of the shell material on the localization of regions of maximum pressure in the fuel is more substantial. In this case (the material 1 is the shell material) in the fuel at the starting stage, two regions of high pressure, attributed to the action of particle 1 and particle 2 are well pronounced. As time passes (Figure 31), the region of high pressure, being formed by particle 1 shifts along X axis -along the line of opposing traffic of particles 1 and 3 to the particle 3. In this case the region, being formed by particle 2, retains its localization.

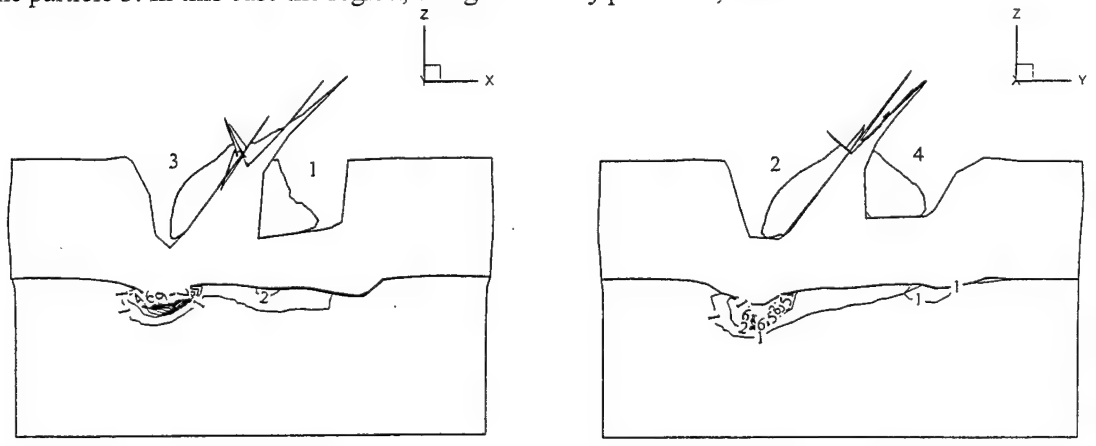


a) b)

Figure 31. Distribution of pressure isolines in cross sections ZX (a) and ZY (b) on different in time impact.Material 1 is the shell material. t=10μsec. 1 - 5GPa, 2 - 9GPa, ..., 10 - 37GPa.

Such asymmetry is explained by interaction of particles between each other, being arised after 6μsec. For the material 2 the localization region of high pressure in the fuel, is close to the localization on simultaneous impact to 10μsec (Figure 32).

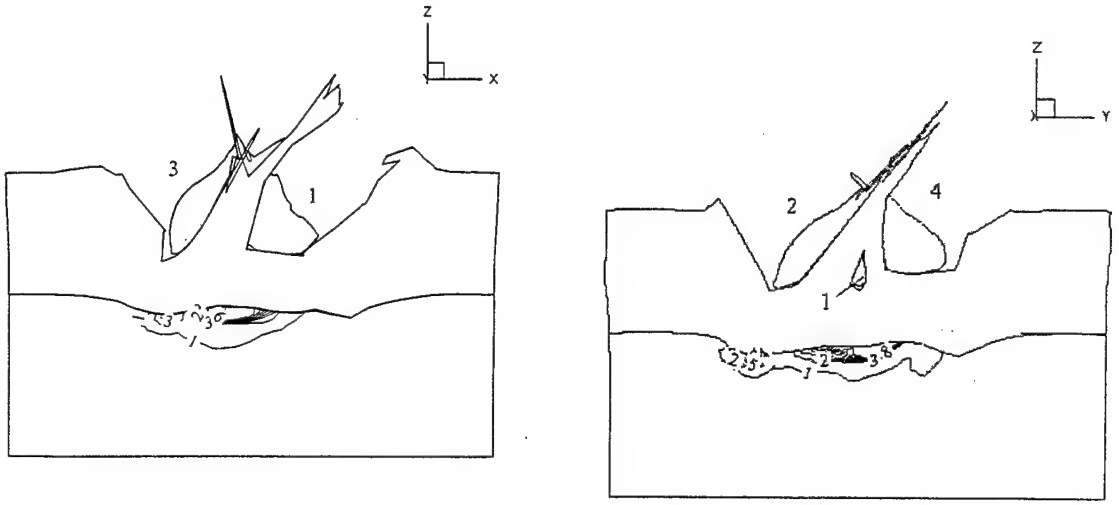


Figure 32. Distribution of pressure isolines in cross sections ZX (a) and ZY (b) on different in time impact.Material 2 is the shell material. t=10μsec. 1 - 1GPa, 2 - 4GPa, ..., 10 - 22GPa.

The degree of mutual influence of particles defines the change in time of coming into the contact with the barriers and can change substantial by the penetration capacity of each of the particle. Changes in time of component velocity of the centre of masses of the particle 1 along axis X ($u_{cm}$) and axis Z ($w_{cm}$) on simultaneous and different in time impact are shown in Figure 33. The particle 1 sharply loses its speed up to 7μsec for $w_{cm}$ and up to 9μsec for $u_{cm}$ on simultaneous impact. Then the picture changes and the retardation is more intense on different in

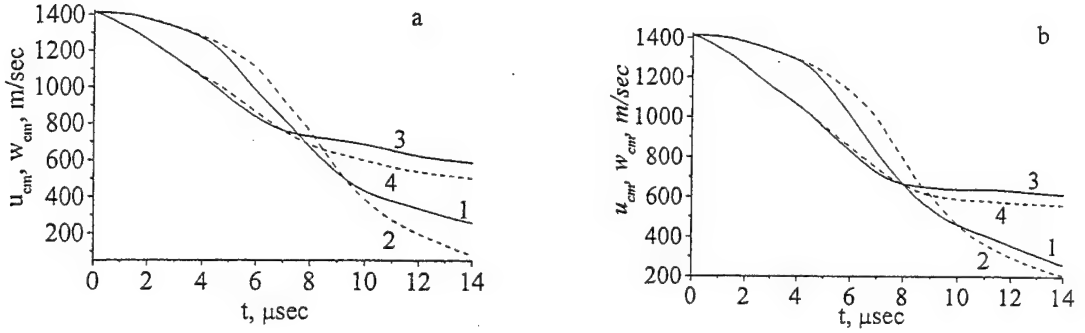


Figure 33. Change in time of component velocity of the centre of masses of particle 1. Curves 1 and 3 - $u_{cm}$ and $w_{cm}$ on simultaneous impact, curves 2 and 4 - $u_{cm}$ and $w_{cm}$ on different in time impact respectively. a - material 1 is the shell material, b - material 2 is the shell material.

time impact. To 14μsec the difference in velocities is 15%and 69% for $w_{cm}$ and $u_{cm}$ respectively. In the case, when the shell is made from the material 2, the difference in corresponding velocities of the particle one is less (Figure 33b) and to 14μsec is 8% for $w_{cm}$ and 14% for $u_{cm}$. In this case the character of change of curves in Figure 33b is similar to the change in Figure 33a.

### 3.5 Pulse Effect

Problems of dynamic deformation of the ball from organoplastic under effect of omnidirectional compression pulse are considered in three–dimensional statement [21]. Homogeneous orthotropic ball with diameter of 10mm was subjected to compression with pulse pressure of 1GPa during 3μsec. It is supposed that the failure of anisotropic material in condition of intense dynamic loads happens in accordance with [3-8]. The material of the ball is the material 1. Already at the time moment of 0.6μsec in ZX cross section (where there is most significant difference between characteristics), the distribution of stress and field of velocities (Figure 35, Figure 36) illustrate the origin of heterogeneous picture of Strain-stress State of the ball. In ZY section the distribution of stress as well as field of velocities is close to one–dimension Strain-stress State of isotropic ball under the effect of omnidirectional compression (Figure 37, Figure 38). At this moment, the stresses achieves maximum values (-2GPa) near at ball poles on Z-axis.

In this case the ball failure arises in the region of maximum stresses. With time the Strain-stress State of anisotropic ball differs from Strain-stress State of isotropic ball more strongly. Isolines of stress and field of rates at the shown in Figure 39 - Figure 41. Evident sliding lines are seen in Figure 39 and Figure 41.

Only $\sigma_x$ distribution in ZY cross section (Figure 408) is closest to the distribution of stress in isotropic ball, maximum stress are achieved in the centers.

Up to 1μsec in all directions, mass velocities are directed into the insight of the ball, but with of 1μsec, in direction X rates change the sign and the increase in ball size begins in this direction. In other directions, mass velocities are directed inside of the ball up to the moment of load removal (3μsec).This, maximum decrease in ball dimensions in X directions is 11% and is achieved to 1μsec, and in Z direction it is 24% and is achieved in 3μsec. Substantial change in the shape of the ball is observed to the moment of cessation of compression pulse action (Figure 42, Figure 43) it acquires dump – bells shape due to the compression along Z axis.

The expansion of the ball in all directions begins after the release of the load. Figure 44 shows the field of velocities in 6μsec, to that moment the material of the ball has been completely failured.

The ball under the effect of omnidirectional compression pulse may transform not to ellipsoid but to the dump – bells under the certain relations of its mechanical characteristics of the value of pressure pulse.

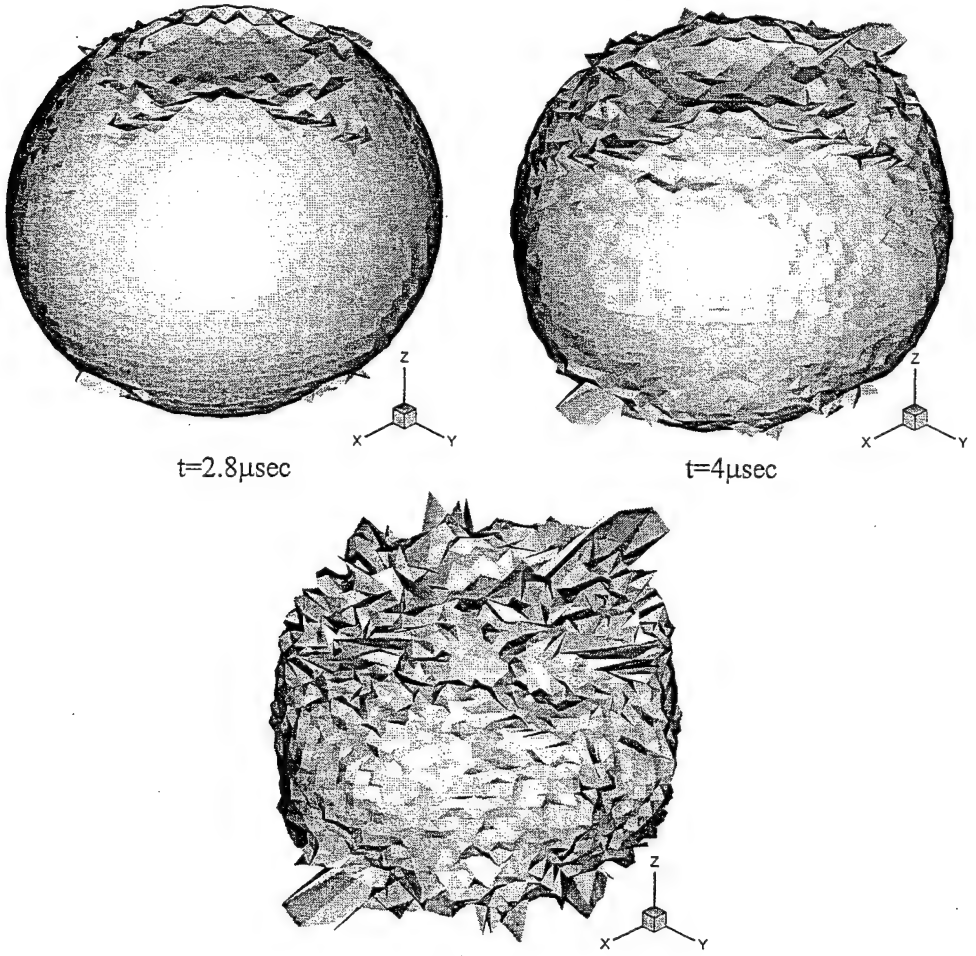


Figure. 34. Volume configurations of orthotropic ball at loading by the pulse of pressure: $P=P_0$ if $t\leq\tau$ and $P=0$ if $t>\tau$. $P_0=1GPa$, $\tau=3\mu sec$.

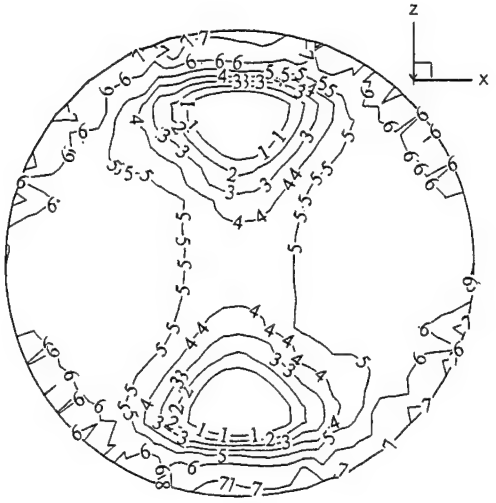


Figure 35. Distribution of isolines of stress $\sigma_x$. t=0.6μsec. 1 - -2GPa, 2 - -1.8GPa, 3 - -1.6GPa, 4 - -1.4GPa, …, 8 - -0.6GPa.

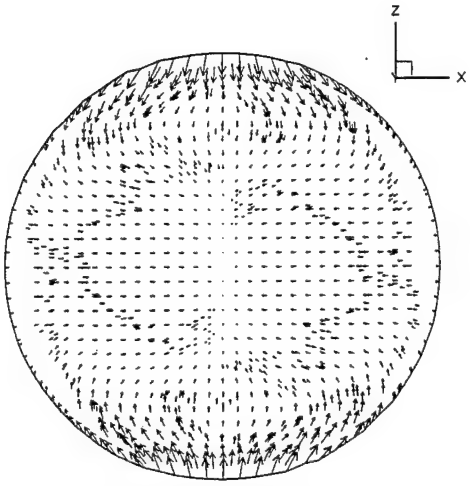


Figure 36. Field of mass velocities. t=0.6μsec.

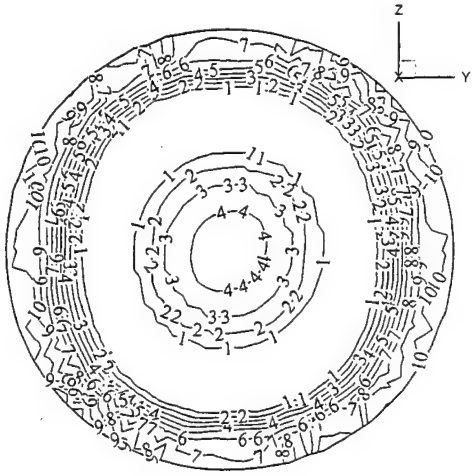


Figure 37. Distribution of isolines of stress $\sigma_x$. t=0.6μsec. 1 - -2GPa, 2 - -1.8GPa, 3 - -1.6GPa, 4 - -1.4GPa, …, 10 - -0.6GPa.

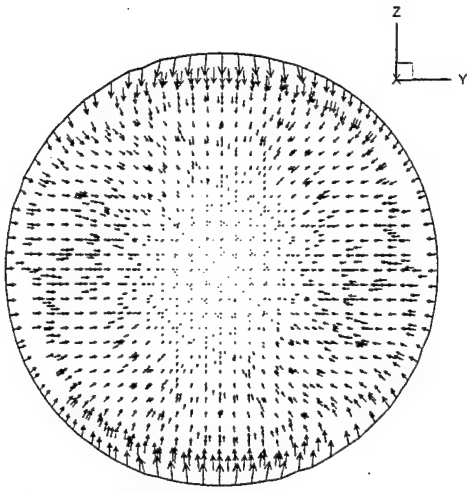


Figure 38. Field of mass velocities. t=0.6μsec.

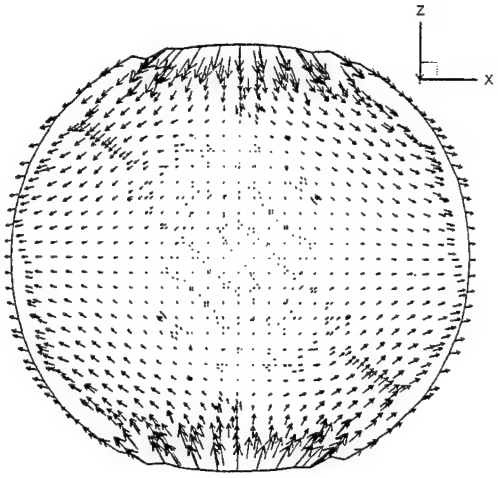


Figure 39. Field of mass velocities. t=1.2μsec.

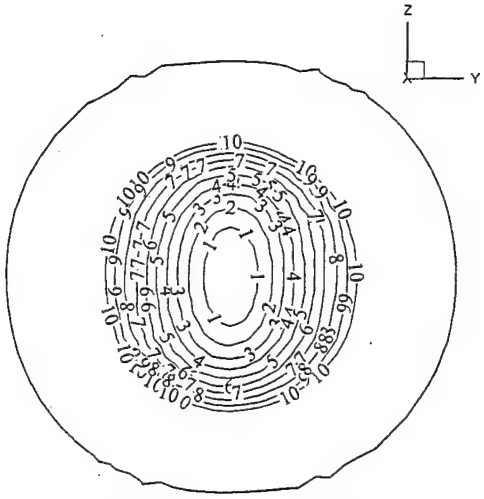


Figure 40. Distribution of isolines of stress $\sigma_x$. t=1.2μsec. 1 - -3GPa, 2 - -2.8GPa, 3 - -2.6GPa, 4 - -2.4GPa, ..., 10 - -1.2GPa.

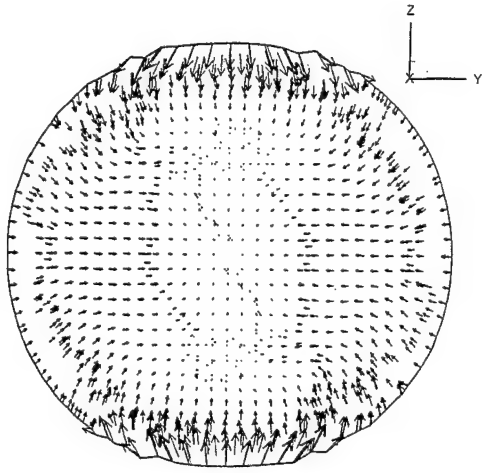


Figure 41. Field of mass velocities. t=1.2μsec.

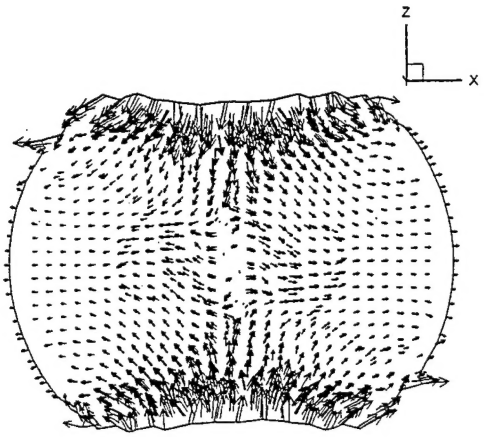


Figure 42. Field of mass velocities. t=3μsec.

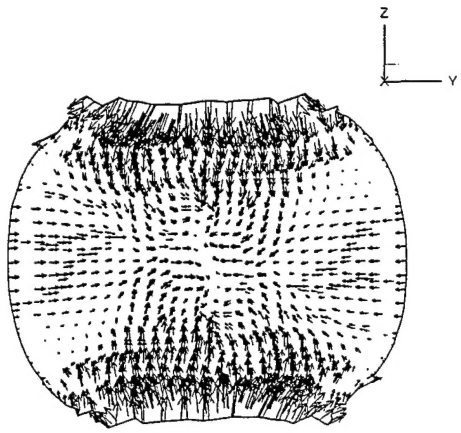


Figure 43. Field of mass velocities. t=3μsec.

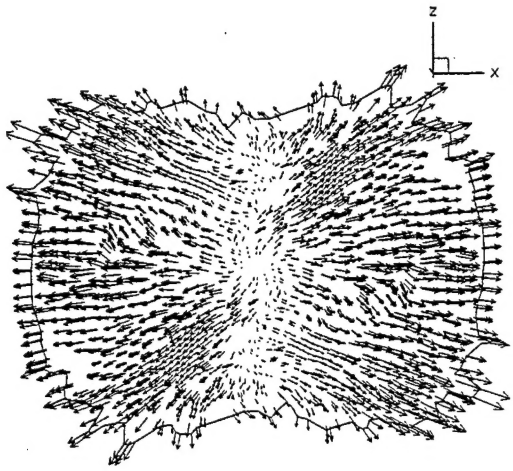


Figure 44. Field of mass velocities. t=6μsec.

## 4 CONCLUSION

1. The offered model allows to describe adequately main laws of the destruction processes of anisotropic materials under dynamic loads. The carried out researches have shown, that anisotropy of properties is the essential factor which is necessary for taking into account for the adequate description and the prediction of development of shock-wave processes and destruction in the materials under dynamic loadings. The influence of anisotropic properties orientation increases with decrease in the velocity interaction.
2. The investigation showed substantial dependence of configurations and volumes of the destruction regions upon the orientation of elastic and strength material properties that defines, as a result, the resistance of the barrier to the penetration in itself.
3. The qualitative and quantitative discrepancies in the destruction of isotropic and anisotropic materials under the dynamic loads are defined not only by strength parameters but either by the interaction of the compression and tension waves. Different speeds of waves propagation along the directions in anisotropic barriers ($C_x=C_y>C_z$ – for transtropic, $C_x>C_y>C_z$ – for orthotropic) provide the discharge of the impact wave and the narrowing in the destruction region.
4. It was stated that the changing orientation of properties causes qualitative changes in mechanisms of macrofailure of anisotropic material.
5. The failure of material 1 occurs due to and during wave processes - it begins in compression wave and completes in reflected relief wave. In material with re-oriented properties (material 2) wave processed don't lead to complete failure. Compression wave destroys the material in upper half of plate, and relief wave causes failures of chipping-off character nearer back surface. In production of striker causes further development of failure in material 2 requires large energy expenses i.e. the most effective protection of the material from impact action may be provided due to the change in properties' orientation.
6. The orientation of material properties of SFRE shell has substantial influence on strain-stress state of fuel on impact and with certain relationships of kinematic and geometric parameters it may became the factor, defining reliability and safety of the construction.

## 5 REFERENCES


1. Wilckins, M. L. "The calculation of elastic-plastic flows." In *Vychislitelniye metody v gidrodinamike,* Mir, Moscow, pp. 212-263, 1967.
2. Bushman, A. V., V. K. Gryaznov, G. I. Kanel, L. A. Ni, S. G. Sugak and V. E. Fortov. "The dynamic of the condensed media under intensive pulse effect. Thermodynamic material properties at high pressures and temperatures." *Preprint, Chernogolovka, OIHF AN USSR,* 1983.
3. Ashkenazi, E. K., and A. V. Ganov. "Anisotropy of the construction materials." *Spravochnik,* Leningrad, 1980.
4. Vu, A. M. "Phenomenological criteria of the destruction of anisotropic media." In *Mehanika kompozicionnyh materialov,* Mir, Moscow, 1985.
5. Radchenko, A. V., and N. K. Galchenko. "The destruction of isotropic and anisotropic steels under dynamic loads." *Fiziko-himicheskaya mehanika materialov*, vol. 28, No. 3, pp. 80-83, 1992.
6. Radchenko, A.V., "Modeling behavior anisotropic of materials at impact." *Mehanika kompozicionih materialov i konstrukciy ( Mechanic of composites and designs)*, vol. 4, No. 4, pp. 51-61, 1998
7. Radchenko, A. V., I. N. Marzenyuk and S. V. Kobenko. "Investigation of Properties of Anisotropic SHS Materials." *4th Int. Symp. on Self - propagation High - temperature Synthesis*, October.6-9, Toledo, Spain, 1997.
8. Radchenko, A. V., I. N. Marzenyuk and S. V. Kobenko. "The influence of heterogeneous materials anisotropy properties on their behaviour under dynamic loads." *V International Conference "Computer-Aided Design of Advanced Materials and Technologies"*, August 4-6, Baikal Lake, Russia, 1997.
9. Johnson, G. R. "Three-dimensional analysis of sliding surface during high velocity impact." *J. Appl. Mech.,* No. 6, pp. 771-773, 1977.
10. Radchenko, A. V. "The application of the finite element method to the calculation of flows in double phase media." In *Chislennye metody mehaniki sploshnoj sredy,* Krasnoyarsk, pp. 106-107, 1989.
11. Johnson, G. R. "High Velocity Impact Calculations in Three Dimension", in *J. Appl. Mech.*, vol. 44, No. 3, pp. 95-100, 1977.
12. Kanel, G.I ., S. V. Razorenov, A. V. Utkin, V. E. Fortov. "Shock wave phenomena in condensed media." M., Yanus-K, 408 p., 1996.
13. Konyaev, A. A., V. F. Tolkachev, A. F. Zorin, A. G. Nazarov. "Measuring calculation complex for recording of dynamic characteristics of the material." *Mathematics modeling of processes in sinergetic systems*, Ulan-Ude – Tomsk, Tomsk University Publishers, pp. 206-208, 1998.
14. Shehter, B. I., L. A. Shushko. "Impact adiabates of some of laminated plastics." *Fizika Goreniya i Vzriava*, vol. 9, No. 9, pp. 599-601, 1973.

15. Radchenko, A. V., S. V. Kobenko. "The dependence of anisotropic material failure on orientation of elastic and strength properties at impact." *Doklady Akademii nauk*, vol. 373, No. 4, pp. 479-482, 2000.

16. Kobenko, S. V., and A. V. Radchenko. "Numeric modeling of deformation and failure of shell construction at impact loads." *Mekhanika kompozicionikh materialov i konstrukciy (Composite Mechanics and Design)*, **5**(1), pp. 3-15, 1999.

17. Radchenko, A. V., and S.V. Kobenko. "Influence of orientation of elastic and strength properties on fracture of orthotropic materials at impact." *Mekhanika kompozicionikh materialov i konstrukciy (Composite Mechanics and Design)*, **5**(4), pp. 8-16, 1999.

18. Radchenko, A. V., S.V. Kobenko, I. N. Marcenuk, I. E. Khorev, G. I. Kanel, V. E. Fortov. "Research on features of behaviour of isotropic and anisotropic materials under impact." *International Journal of Impact Engineering*, **23**(1-10), pp. 745-756, 1999.

19. Kanel, G. I., and V. V. Zherban. "Elastic deformation and chipping-of failure of iron "Armko" in the shock-wave." *Fiz. Gor. Vzryva*, **16**(4), pp. 93-103, 1980.

20. Radchenko A. V., Kobenko S. V., Krivosheina M. N. "Modeling impacting loading of solid fuel fastened with the orthotropic shell" *Mekhanika kompozicionikh materialov i konstrukciy (Composite Mechanics and Design)*, vol. 6, No. 3, pp. 343-358, 2000.

21. Krivosheina M. N., Radchenko, A. V., Kobenko S. V. "Destruction orthotropic and isotropic spherical bodies under action of a pulse of all-round compression" *Mekhanika kompozicionikh materialov i konstrukciy (Composite Mechanics and Design)*, vol. 7, No. 1, pp. 95-102, 2001.

22. Radchenko A. V., Krivosheina M. N., Kobenko S.V., Marcenuk I. N. "Influence of properties anisotropy of the shell on initiation of a detonation in solid fuel at impact and pulse loadings" *Khimicheskay fizika (Chemical physics)*, vol. 20, No. 6, pp. 123-128, 2001.

23. Radchenko A. V., Kobenko S.V., Tolkachev V. F. "The experimental and numerical analysis of a wave picture in the anisotropic material at impact" *"Extreme states of substance. Detonation. Shock waves". International conference III Khariton's topical scientific readings (Sarov, February 26 – March 2 2001) – RFNC-VNIIEF,* pp.124-125., 2001.